

## AVERAGING TECHNIQUES FOR THE EFFECTIVE NUMERICAL SOLUTION OF SYMM'S INTEGRAL EQUATION OF THE FIRST KIND\*

CARSTEN CARSTENSEN<sup>†</sup> AND DIRK PRAETORIUS<sup>‡</sup>

**Abstract.** Averaging techniques for finite element error control, occasionally called *ZZ estimators* for the gradient recovery, enjoy a high popularity in engineering because of their striking simplicity and universality: One does not even require a PDE to apply the nonexpensive post-processing routines. Recently, averaging techniques have been mathematically proved to be reliable and efficient for various applications of the finite element method. This paper establishes a class of averaging error estimators for boundary integral methods. Symm's integral equation of the first kind with a nonlocal single-layer integral operator serves as a model equation studied both theoretically and numerically. We introduce four new error estimators which are proven to be reliable and efficient up to terms of higher order. The higher-order terms depend on the regularity of the exact solution. Several numerical experiments illustrate the theoretical results and show that the [normally unknown] error is sharply estimated by the proposed estimators, i.e., error and estimators almost coincide.

**Key words.** integral equations, boundary element method, a posteriori error estimates, reliability, efficiency, adaptive algorithm

**AMS subject classifications.** 65N38, 65R20, 65N50

**DOI.** 10.1137/040609033

**1. Introduction.** Reliable error control and efficient meshdesign in today's boundary element analysis are usually based on a posteriori error estimates. Let  $\Omega$  be a bounded domain in  $\mathbb{R}^d$ ,  $d = 2, 3$ , with Lipschitz boundary  $\partial\Omega$ , and let  $\Gamma \subset \partial\Omega$  be an open surface. Suppose we are given the right-hand side  $f$  and an approximation  $u_h$  for the unknown exact solution  $u$  of the operator equation

$$(1.1) \quad Vu = f \quad \text{in } \tilde{H}^{-1/2}(\Gamma)$$

for the single-layer potential [ $ds_y$  denotes surface integration on  $\Gamma \subseteq \mathbb{R}^d$  with respect to the variable  $y$ ] defined by

$$(1.2) \quad (Vu)(x) = \int_{\Gamma} u(y)\kappa(x-y) ds_y \quad \text{for } x \in \Gamma$$

and interpreted in a weak sense for the kernel

$$(1.3) \quad \kappa(x) := \begin{cases} -\frac{1}{\pi} \log |x| & \text{for } d = 2, \\ \frac{1}{2\pi} |x|^{-1} & \text{for } d = 3. \end{cases}$$

A posteriori error estimators  $\eta = \eta(u_h, f, T)$  are computable quantities in terms of the right-hand side  $f$ , a computed approximate solution  $u_h$ , and the given underlying

---

\*Received by the editors May 26, 2004; accepted for publication (in revised form) March 8, 2005; published electronically January 6, 2006. The support of the Austrian Science Fund FWF under grant P15274 is thankfully acknowledged.

<http://www.siam.org/journals/sisc/27-4/60903.html>

<sup>†</sup>Department of Mathematics, Humboldt-Universität zu Berlin, Unter den Linden 6, D-10099 Berlin, Germany (cc@math.hu-berlin.de).

<sup>‡</sup>Institute for Analysis and Scientific Computing, Vienna University of Technology, Wiedner Hauptstrasse 8-10, A-1040 Vienna, Austria (Dirk.Praetorius@tuwien.ac.at).

mesh  $\mathcal{T} = \{\Gamma_1, \dots, \Gamma_n\}$  which bound the exact error from below or above [so-called efficiency and reliability of  $\eta$ , resp.]. So far, for boundary element methods, the following four groups (i)–(iv) of a posteriori estimates have been introduced; see [CFa] for more details.

(i) Weighted residual error estimators in 2D, established in [C1, C2, C3, CES, CS1, CS2],

$$(1.4) \quad \eta_{R,j} := h_j^\alpha \|\partial R/\partial s\|_{L^2(\Gamma_j)}$$

with the derivative  $\partial R/\partial s$  of the residual  $R := f - Vu_h$  along  $\Gamma$  and  $h_j := |\Gamma_j|$  the size of  $\Gamma_j$ . For the  $hp$ -method, see [CFS] and, recently, for 3D [CMS, CMPS].

(ii) Local double-integral seminorms in [F2, F3, CP1] with a double integration over overlapping domains  $\omega_j := \Gamma_{j-1} \cup \Gamma_j$  in 2D and 3D,

$$(1.5) \quad \varrho_{F,j}^2 := \int_{\omega_j} \int_{\omega_j} \frac{|R(x) - R(y)|^2}{|x - y|^{1+2\alpha}} ds_x ds_y.$$

(iii) Based on an idea in the finite element literature [BR], Babuška–Rheinboldt-type error estimators are suggested in [F1], so far only for hypersingular integral equations.

(iv) Multilevel error estimators involve a hierarchy of grids and, usually, a disputable saturation assumption [MMS, MSW, CMPS].

Other suggested error estimators employ the notion of an influence index and strengthened Cauchy inequalities [R1, R2, WY, Y1, Y2], localize the outer integration in the Sobolev–Slobodeckij norm (1.5) of the residual  $R := f - Vu_h$  [FHK], try to recover gradients [SW, SSW], or employ corrections with another integral equation [MPM, S, SSt].

The nonlocal character of the involved pseudodifferential operator  $V$  and the nonlocal Sobolev spaces [of functions on  $\Gamma$ ] cause severe difficulties in the mathematical derivation of computable lower and upper error bounds for a discrete (known) approximation  $u_h$  to the (unknown) exact solution  $u$ . A comparison [F2, F3] shows that the Faermann error estimator  $\eta_F := (\sum_{j=1}^n \eta_{F,j}^2)^{1/2}$  and its modification  $\mu_F$  from [CP1] were the *only* proven reliable and efficient estimators for unstructured grids in the sense that

$$(1.6) \quad C_{\text{eff}} \|u - u_h\|_{\tilde{H}^{-1/2}(\Gamma)} \leq \eta_F \leq \mu_F \leq C_{\text{rel}} \|u - u_h\|_{\tilde{H}^{-1/2}(\Gamma)}$$

for the energy norm  $\|u - u_h\|_{\tilde{H}^{-1/2}(\Gamma)}$  of the error in a Galerkin boundary element method.

In this paper we introduce a new class of error estimators  $\eta_M, \mu_M, \eta_A$ , and  $\mu_A$  for Symm's integral equation based on averaging techniques. For finite element methods it has recently been shown that any averaging technique yields in fact reliable error estimators [ZZ, CB, AC, CFu]. Our results in this paper establish this concept for the Galerkin boundary element method.

In the simplest case, let  $\mathcal{T}_H$  be a given mesh with mesh size  $H$ , and let  $\mathcal{T}_h$  be obtained by uniform refinements of  $\mathcal{T}_H$ . Let  $u_h \in \mathcal{P}_0(\mathcal{T}_h)$  be a  $\mathcal{T}_h$ -piecewise constant Galerkin approximation of the exact solution  $u \in \tilde{H}^{-1/2}(\Gamma)$  of (1.1). If  $\mathbb{G}_H : \tilde{H}^{-1/2}(\Gamma) \rightarrow \mathcal{P}_1(\mathcal{T}_H)$  and  $\mathcal{A}_H : \tilde{H}^{-1/2}(\Gamma) \rightarrow \mathcal{P}_1(\mathcal{T}_H)$  denote the Galerkin projection, respectively, the  $L^2$ -projection onto the  $\mathcal{T}_H$ -piecewise affine [not necessarily continuous] functions and if the mesh size  $h$  is small enough compared with  $H$ , then the error estimator [with  $\|\cdot\|$  the energy norm of section 2.2]

$$(1.7) \quad \eta_M := \|u_h - \mathbb{G}_H u_h\| := \langle V(u_h - \mathbb{G}_H u_h); u_h - \mathbb{G}_H u_h \rangle^{1/2}$$

is always reliable and efficient up to terms of higher order; cf. Theorem 5.2. The higher-order terms depend only on the smoothness of the exact solution  $u \in \tilde{H}^{-1/2}$ . For the lowest-order ansatz  $u_h \in \mathcal{P}_0(\mathcal{T}_h)$  it suffices that  $u$  is  $\mathcal{T}_h$ -piecewise in  $H^{1+\varepsilon}$  for some  $\varepsilon > 0$  [in fact,  $\Gamma$  is therefore required to be piecewise smoother than only Lipschitz].

Since  $\mathbb{G}_H$  is the best approximation operator with respect to the energy norm, there holds  $\|u_h - \mathbb{G}_H u_h\| \leq \|u_h - \mathcal{A}_H u_h\|$ . In particular, the error estimator

$$(1.8) \quad \eta_A := \|u_h - \mathcal{A}_H u_h\|$$

is reliable. Theorem 5.6 states the efficiency of  $\eta_A$  provided  $H^1$ -stability of  $\mathcal{A}_H$  [i.e.,  $\mathcal{A}_H$  is continuous as operator from  $H^1(\Gamma)$  to  $H^1(\Gamma)$ ]. By interpolation and inverse estimates we show that the error estimators

$$(1.9) \quad \mu_M := \|H^{1/2}(\mathbb{1} - \mathbb{G}_H)u_h\|_{L^2(\Gamma)} \quad \text{and} \quad \mu_A := \|H^{1/2}(\mathbb{1} - \mathcal{A}_H)u_h\|_{L^2(\Gamma)}$$

are equivalent to  $\eta_M$  and  $\eta_A$ , respectively, i.e.,

$$(1.10) \quad C_1^{-1} \mu_M \leq \eta_M \leq C_2 \mu_M \quad \text{and} \quad C_1^{-1} \mu_A \leq \eta_A \leq C_2 \mu_A$$

with constants  $C_1, C_2$  that do not depend on the size or the number of the elements in  $\mathcal{T}_h$  and  $\mathcal{T}_H$ ; cf. Corollaries 5.4 and 5.5. Since the  $L^2$  norm is local in the sense that  $\|\cdot\|_{L^2(\Gamma)}^2 = \sum_{\gamma \in \mathcal{T}_H} \|\cdot\|_{L^2(\gamma)}^2$ ,  $\mu_M$  and  $\mu_A$  can be employed for an indicator-based adaptive mesh refinement introduced in section 6.3 below.

The paper is organized as follows: section 2 recalls the definition of the Sobolev spaces  $\tilde{H}^\alpha(\Gamma)$  and  $H^\alpha(\Gamma)$  of fractional order  $-1 \leq \alpha \leq 1$ . Section 3 displays preliminaries on the mesh geometry and finite elements. A local first-order approximation result for the  $L^2$ -projection in scales of  $H^\alpha(\Gamma)$  is proven in section 4. Section 5 establishes the a posteriori error estimates and introduces four error estimators (1.7)–(1.9) based on averaging techniques. In section 6 we give implementational details following the spirit of [CP1]. Finally, section 7 reports on five experiments, from which conclusions are drawn in section 8.

**2. Preliminaries on the functional analytic setting.** This section aims to recall the definition of the fractional-order Sobolev spaces on open screens  $\Gamma \subseteq \partial\Omega$ , where  $\Omega$  is a bounded Lipschitz domain in  $\mathbb{R}^d$ ,  $d = 2, 3$ , with boundary  $\partial\Omega$ . We provide the interpolation results we are going to use in section 4 and recall the mapping properties of the single layer potential (1.2) in scales of Sobolev spaces  $H^\alpha(\Gamma)$ .

**2.1. Fractional order Sobolev spaces and interpolation.** For any (relatively) open set  $\omega \subseteq \partial\Omega$  and  $0 \leq \alpha \leq 1$ , we define Sobolev spaces of fractional order by complex interpolation

$$(2.1) \quad \tilde{H}^\alpha(\omega) = [L^2(\omega); H_0^1(\omega)]_\alpha \quad \text{and} \quad H^\alpha(\omega) = [L^2(\omega); H^1(\omega)]_\alpha,$$

where  $[X_0; X_1]_\alpha$  denotes the complex interpolation of  $X_0$  and  $X_1 \subseteq X_0$  [BL, McL]. The norm  $\|\cdot\|_{H^1(\omega)}$  is given by the surface gradient  $\nabla$  as  $\|u\|_{H^1(\omega)}^2 = \|u\|_{L^2(\omega)}^2 + \|\nabla u\|_{L^2(\omega)}^2$ , and  $H^1(\omega)$  and  $H_0^1(\omega)$  are defined as the completions of  $\text{Lip}(\omega)$  and  $\{v \in \text{Lip}(\omega) : v|_{\partial\omega} = 0\}$ , respectively. Sobolev spaces with negative index are defined by duality,

$$(2.2) \quad H^{-\alpha}(\Gamma) := \tilde{H}^\alpha(\Gamma)^* \quad \text{and} \quad \tilde{H}^{-\alpha}(\Gamma) := H^\alpha(\Gamma)^*$$

with corresponding norms and duality brackets

$$(2.3) \quad \langle \cdot; \cdot \rangle \quad \text{in } \tilde{H}^{-\alpha}(\Gamma) \times H^\alpha(\Gamma)$$

which extend the  $L^2(\Gamma)$  scalar product.

*Remark 2.1.* Let  $X_0, X_1$  be normed spaces with  $X_1 \subseteq X_0$  and  $0 \leq \alpha \leq 1$ . Then, the norm of the interpolation space  $X := [X_0; X_1]_\alpha$  satisfies

$$(2.4) \quad \|\cdot\|_{[X_0; X_1]_\alpha} \leq \|\cdot\|_{X_0}^{1-\alpha} \|\cdot\|_{X_1}^\alpha.$$

Furthermore, let  $Y := [Y_0; Y_1]_\alpha$  be the complex interpolation of normed spaces  $Y_1 \subseteq Y_0$ . If  $T \in L(X_0; Y_0)$  can also be viewed as an operator  $T \in L(X_1; Y_1)$ , then  $T : X \rightarrow Y$  is well defined and continuous and the corresponding operator norms satisfy

$$(2.5) \quad \|T\|_{L(X; Y)} \leq \|T\|_{L(X_0; Y_0)}^{1-\alpha} \|T\|_{L(X_1; Y_1)}^\alpha. \quad \square$$

**LEMMA 2.1** (see [P, StS]). *Let  $\mathcal{T} = \{\Gamma_1, \dots, \Gamma_n\}$  be a partition of  $\Gamma$  into elements  $\Gamma_1, \dots, \Gamma_n$ . For  $0 \leq \alpha \leq 1$  and  $u \in H^\alpha(\Gamma)$ , we have  $u|_{\Gamma_j} \in H^\alpha(\Gamma_j)$  for all  $j = 1, \dots, n$  with*

$$(2.6) \quad \sum_{j=1}^n \|u|_{\Gamma_j}\|_{H^\alpha(\Gamma_j)}^2 \leq \|u\|_{H^\alpha(\Gamma)}^2. \quad \square$$

*Remark 2.2.* (i) The constant factor 1 on the right-hand side of (2.6) [not displayed explicitly] holds for complex interpolation and needs to be replaced by an  $n$ -independent constant in case of real interpolation as well as in case of alternative definitions by extension or by Sobolev–Slobodeckij norms.

(ii) The converse inequality in (2.6) fails to hold in general [F2, F3].

**2.2. Single-layer potential and energy norm.** The single-layer potential (1.2) defines a continuous linear operator

$$(2.7) \quad V : \tilde{H}^{\alpha-1}(\Gamma) \rightarrow H^\alpha(\Gamma)$$

for all  $0 \leq \alpha \leq 1$  [Co, McL]. For  $d = 3$ ,  $V$  always is an isomorphism [i.e.,  $V$  is bijective and  $V$  and  $V^{-1}$  are continuous]. Moreover,

$$(2.8) \quad \langle u; v \rangle := \langle Vu; v \rangle \quad \text{for } u, v \in \tilde{H}^{-1/2}(\Gamma)$$

defines a scalar product on  $\tilde{H}^{-1/2}(\Gamma)$ . For  $d = 2$ ,  $V$  is bijective if the capacity of  $\Gamma$  is not 1, and (2.8) defines a scalar product on  $\tilde{H}^{-1/2}(\Gamma)$  provided the capacity is strictly less than 1 [e.g.,  $\Omega$  is contained in the open unit disk]; cf. [McL].

In what follows we assume for  $d = 2$  that the capacity of  $\Omega$  is strictly less than 1 so that all results of this paper hold for  $d = 2$  and  $d = 3$  simultaneously. The induced *energy norm*

$$(2.9) \quad \|u\| := \langle u; u \rangle^{1/2}$$

is an equivalent norm on  $\tilde{H}^{-1/2}(\Gamma)$ . According to the Lax–Milgram lemma, given  $f \in H^{1/2}(\Gamma)$  there is a unique solution  $u := V^{-1}f \in \tilde{H}^{-1/2}(\Gamma)$  of (1.1).

**3. Preliminaries on finite element approximation.**

**3.1. Galerkin discretization of  $\widetilde{H}^{-1/2}(\Gamma)$ .** Let  $\mathcal{T} = \{\Gamma_1, \dots, \Gamma_n\}$  be a triangulation of  $\Gamma$ . Each element  $\Gamma_j$  of the triangulation  $\mathcal{T}$  is supposed to be a connected (affine) boundary piece for  $d = 2$  and a (flat) triangle for  $d = 3$ , respectively. For  $d = 3$ , we assume that  $\mathcal{T}$  is a regular triangulation: Two distinct and intersecting  $\Gamma_j$  and  $\Gamma_k$  share either a common edge or a vertex. The set of all nodes of the triangulation  $\mathcal{T}$  is denoted with  $\mathcal{N}$ . Let  $h \in L^\infty(\Gamma)$  denote the local mesh size  $h|_{\Gamma_j} := h_j := \text{diam}(\Gamma_j)$ .

For an integer  $p \geq 0$ ,  $\mathcal{P}_p(\mathcal{T})$  denotes the space of all isoparametric polynomials of total degree  $\leq p$  [defined on reference elements  $\Gamma_{\text{ref}} = [0, 1]$  and  $\Gamma_{\text{ref}} = \text{conv}\{(0, 0), (0, 1), (1, 0)\}$  for  $d = 2, 3$ , resp.].

If  $\mathcal{S}$  is a finite dimensional subspace of  $\widetilde{H}^{-1/2}(\Gamma)$  [e.g.,  $\mathcal{S} = \mathcal{P}_p(\mathcal{T})$ ], the discrete Galerkin approximation  $u_h \in \mathcal{S}$  is uniquely determined by the linear system of equations

$$(3.1) \quad \langle u_h; v_h \rangle = \langle f; v_h \rangle \quad \text{for all } v_h \in \mathcal{S}.$$

The Galerkin projection  $\mathbb{G} : \widetilde{H}^{-1/2}(\Gamma) \rightarrow \mathcal{S}$  defined by

$$\langle \mathbb{G}u; v_h \rangle = \langle u; v_h \rangle \quad \text{for all } v_h \in \mathcal{S}$$

is the orthogonal projection onto  $\mathcal{S} \subseteq \widetilde{H}^{-1/2}(\Gamma)$  with respect to the energy norm.

**3.2. Inverse estimate for the energy norm.** Given  $\mathcal{T}$  and  $\mathcal{S} = \mathcal{P}_p(\mathcal{T})$ , we assume that there is a mesh size independent constant  $C_{\text{inv}} > 0$  which depends only on  $\Gamma$ ,  $p$ , and the shape of the elements of  $\mathcal{T}$  such that, for all  $v_h \in \mathcal{P}_p(\mathcal{T})$ , there holds

$$(3.2) \quad \|v_h\|_{L^2(\Gamma)} \leq C_{\text{inv}} \|h^{-1/2}v_h\|.$$

*Remark 3.1.* The estimate (3.2) is proven in [GHS, Theorem 3.6] for  $p \in \mathbb{N}_0$  and  $\Gamma$  a 2D manifold in  $\mathbb{R}^3$ , but the arguments work for a 1D boundary as well. We stress that here, with a focus on adapted meshes, the *local* mesh size enters the estimates. Well-established inverse estimates

$$(3.3) \quad \|v_h\|_{L^2(\Gamma)} \lesssim h_{\min}^{-1/2} \|v_h\| \quad \text{for } v_h \in \mathcal{P}_p(\mathcal{T})$$

involve the global quantity  $h_{\min} := \min_{1 \leq j \leq n} h_j$ .

**3.3. Standard approximation estimate.** Given a regular triangulation  $\mathcal{T}$ , real numbers  $\alpha, m \in \mathbb{R}$  with  $m \geq \alpha$ , and an integer  $p \geq 0$ , define  $\widehat{p} := \min\{p+1, m\} - \alpha$ . Moreover, let  $\mathcal{S}_p(\mathcal{T})$  denote either  $\mathcal{P}_0(\mathcal{T})$  or  $\mathcal{P}_p(\mathcal{T}) \cap \mathcal{C}(\Gamma)$  for  $p = 0$  and  $p > 0$ , respectively. Define the  $\mathcal{T}$ -piecewise Sobolev space

$$H^m(\mathcal{T}) := \{u \in L^2(\Gamma) : u|_{\Gamma_j} \in H^m(\Gamma_j) \text{ for all } \Gamma_j \in \mathcal{T}\}$$

with norm  $\|u\|_{H^m(\mathcal{T})}^2 = \sum_{j=1}^n \|u|_{\Gamma_j}\|_{H^m(\Gamma_j)}^2$ . Then, there is constant  $C_3 > 0$  depending only on  $\Gamma, \alpha, m, p$ , and the shape of the elements in  $\mathcal{T}$  such that

$$(3.4) \quad \min_{v_h \in \mathcal{S}_p(\mathcal{T})} \|u - v_h\|_{H^\alpha(\Gamma)} \leq C_3 h_{\max}^{\widehat{p}} \|u\|_{H^m(\mathcal{T})}$$

for all  $u \in H^\alpha(\Gamma) \cap H^m(\mathcal{T})$  and  $h_{\max} := \max_{1 \leq j \leq n} h_j$ ; cf. [SaS].

**3.4. Local first-order approximation operator.** The following definitions adapt [CB] for fixed  $0 \leq \alpha \leq 1$  to obtain an approximation operator:

$$(3.5) \quad \mathcal{J}_h : H^\alpha(\Gamma) \rightarrow \mathcal{P}_1(\mathcal{T}) \cap \mathcal{C}(\Gamma) \subseteq L^2(\Gamma).$$

For each node  $z \in \mathcal{N}$  let  $\varphi_z \in \mathcal{P}_1(\mathcal{T}) \cap \mathcal{C}(\Gamma)$  denote the nodal basis functions with  $\varphi_z(z) = 1$  and  $\varphi_z(\tilde{z}) = 0$  for  $\tilde{z} \in \mathcal{N} \setminus \{z\}$ . Note that  $\{\varphi_z : z \in \mathcal{N}\}$  is a partition of unity. The support of  $\varphi_z$  is denoted with  $\omega_z := \text{supp}(\varphi_z)$  and has the diameter  $h_z := \text{diam}(\omega_z)$ . For each  $u \in L^1(\Gamma)$  define

$$(3.6) \quad \mathcal{J}_h(u) := \sum_{z \in \mathcal{N}} \lambda_z(u) \varphi_z \in \mathcal{P}_1(\mathcal{T}) \cap \mathcal{C}(\Gamma) \quad \text{with} \quad \lambda_z(u) := \frac{\int_{\omega_z} u \varphi_z \, ds}{\int_{\omega_z} \varphi_z \, ds}$$

for  $z \in \mathcal{N}$ .

LEMMA 3.1. *There is a constant  $C_4 > 0$  that depends on  $\Gamma$  and the aspect ratio of the elements [but not on their sizes] such that for all  $z \in \mathcal{N}$ ,  $0 \leq \alpha \leq 1$ , and  $u \in H^\alpha(\Gamma)$  there holds*

$$(3.7) \quad \|(u - \lambda_z(u))\varphi_z\|_{L^2(\omega_z)} \leq C_4 h_z^\alpha \|u\|_{H^\alpha(\omega_z)}.$$

*Proof.* We derive from [CB, Theorem 2.1] the existence of  $C_4 > 0$  such that

$$\|(u - \lambda_z(u))\varphi_z\|_{L^2(\omega_z)} \leq C_4 \min\{\|u\|_{L^2(\omega_z)}, h_z \|\nabla u\|_{L^2(\omega_z)}\}$$

for all  $z \in \mathcal{N}$  and  $u \in H^1(\Gamma)$ . [The proof therein is formulated for a domain  $\Gamma \subseteq \mathbb{R}^2$  but applies to the present situation.] For  $\alpha = 0$  and  $\alpha = 1$ , the linear operator

$$T_\alpha : H^\alpha(\omega_z) \rightarrow L^2(\omega_z), u \mapsto (u - \lambda_z(u))\varphi_z$$

is well defined and continuous with operator norms  $\|T_0\| \leq C_4$  and  $\|T_1\| \leq C_4 h_z$ , respectively. By interpolation,  $T_\alpha$  is well defined and continuous with  $\|T_\alpha\| \leq C_4 h_z^\alpha$ . This proves (3.7).  $\square$

**4. Local first-order approximation property.** An interpolation argument shows that the  $L^2$ -projection has a local first-order approximation property with respect to the energy norm [equivalent to the  $\tilde{H}^{-1/2}$  norm].

DEFINITION 1. *Let  $\mathcal{S}$  be a subspace of  $\mathcal{P}_p(\mathcal{T})$ ,  $p \geq 0$ . For  $0 \leq \alpha \leq 1$ , a [not necessarily linear] mapping  $\mathcal{A} : L^2(\Gamma) \rightarrow \mathcal{S}$  has a local first-order approximation property with respect to the  $\tilde{H}^{-\alpha}$ -norm, if there is a constant  $C_{\text{apx}} > 0$  which exclusively depends on  $\Gamma$ ,  $\alpha$ ,  $p$ , and the shape of the elements in  $\mathcal{T}$ , such that the following estimate holds,*

$$(4.1) \quad \|(\mathbb{1} - \mathcal{A})v\|_{\tilde{H}^{-\alpha}(\Gamma)} \leq C_{\text{apx}} \|h^\alpha v\|_{L^2(\Gamma)} \quad \text{for all } v \in L^2(\Gamma).$$

*In particular, the constant  $C_{\text{apx}}$  is assumed to be independent of number and size of the elements.*

The following theorem shows that the  $L^2$ -projection has the first-order approximation property provided the space  $\mathcal{S}$  is rich enough. It will be used first to prove reliability and efficiency of  $\eta_M$  in Theorem 5.1 and second to show reliability of  $\mu_A$  and  $\mu_M$  in Corollary 5.4.

THEOREM 4.1. *Suppose that  $\mathcal{S}$  contains  $\mathcal{P}_0(\mathcal{T})$  or  $\mathcal{P}_1(\mathcal{T}) \cap \mathcal{C}(\Gamma)$ . Then, the  $L^2$ -projection  $\Pi : L^2(\Gamma) \rightarrow \mathcal{S}$  onto  $\mathcal{S}$  has the local first-order approximation property (4.1).*

The proof of Theorem 4.1 follows ideas from [CMPS, Theorem 4.1] and involves Lemmas 2.1 and 3.1. We shall consider the cases  $\mathcal{P}_0(\mathcal{T}) \subseteq \mathcal{S}$  and  $\mathcal{P}_1(\mathcal{T}) \cap \mathcal{C}(\Gamma) \subseteq \mathcal{S}$  separately.

*Proof of Theorem 4.1 in case  $\mathcal{P}_1(\mathcal{T}) \cap \mathcal{C}(\Gamma) \subseteq \mathcal{S}$ .* Notice that, for  $v \in L^2(\Gamma)$ , orthogonality of the projection  $(\mathbb{1} - \Pi)$  and  $\varphi_z \in \mathcal{S}$  lead to

$$(4.2) \quad \langle (\mathbb{1} - \Pi)v; \varphi_z \rangle = 0 \quad \text{for all } z \in \mathcal{N}.$$

For  $u \in H^\alpha(\Gamma)$ , we have  $u = \sum_{z \in \mathcal{N}} u \varphi_z$  and therefore  $\varrho := (\mathbb{1} - \Pi)v$  satisfies

$$(4.3) \quad \begin{aligned} \langle \varrho; u \rangle &= \sum_{z \in \mathcal{N}} \langle \varrho; u \varphi_z \rangle = \sum_{z \in \mathcal{N}} \langle \varrho; (u - \lambda_z(u)) \varphi_z \rangle \\ &\leq \sum_{z \in \mathcal{N}} \|\varrho\|_{L^2(\omega_z)} \|(u - \lambda_z(u)) \varphi_z\|_{L^2(\omega_z)}. \end{aligned}$$

The combination of (4.3) and (3.7) yields

$$(4.4) \quad \begin{aligned} \langle \varrho; u \rangle &\leq C_4 \sum_{z \in \mathcal{N}} \|h_z^\alpha \varrho\|_{L^2(\omega_z)} \|u\|_{H^\alpha(\omega_z)} \\ &\leq C_4 \left( \sum_{z \in \mathcal{N}} \|h_z^\alpha \varrho\|_{L^2(\omega_z)}^2 \right)^{1/2} \left( \sum_{z \in \mathcal{N}} \|u\|_{H^\alpha(\omega_z)}^2 \right)^{1/2}. \end{aligned}$$

A coloring argument in [CMS, section 3] and [CMPS, Theorem 4.1] shows that we can find a finite number of index sets  $J_1, J_2, \dots, J_M$  such that for each  $k$  the sets  $\omega_z$  in  $\{ \omega_z : z \in J_k \}$  are pairwise disjoint. The number  $M$  depends on the overlap of the patches  $\omega_z, z \in \mathcal{N}$ , and thus on the aspect ratios of the elements and on  $\Gamma$ . Lemma 2.1 can be applied for each set  $J_k$  and so yields eventually

$$(4.5) \quad \sum_{z \in \mathcal{N}} \|u\|_{H^\alpha(\omega_z)}^2 \leq M \|u\|_{H^\alpha(\Gamma)}^2.$$

With the constant  $C_5 := \max\{h_z/h_T : z \in \mathcal{K}, T \in \mathcal{T} \text{ with } T \subseteq \omega_z\}$ , there holds

$$(4.6) \quad \sum_{z \in \mathcal{N}} \|h_z^\alpha \varrho\|_{L^2(\omega_z)}^2 \leq C_5^{2\alpha} \sum_{z \in \mathcal{N}} \|h^\alpha \varrho\|_{L^2(\omega_z)}^2 \leq M C_5^{2\alpha} \|h^\alpha \varrho\|_{L^2(\Gamma)}^2.$$

The combination of (4.4), (4.6) yields

$$(4.7) \quad \|\varrho\|_{\tilde{H}^{-\alpha}(\Gamma)} = \sup_{\substack{u \in H^\alpha(\Gamma) \\ u \neq 0}} \frac{\langle \varrho; u \rangle}{\|u\|_{H^\alpha(\Gamma)}} \leq M C_4 C_5^\alpha \|h^\alpha \varrho\|_{L^2(\Gamma)}. \quad \square$$

*Proof of Theorem 4.1 in case  $\mathcal{P}_0(\mathcal{T}) \subseteq \mathcal{S}$ .* With  $\Pi_0 : L^2(\Gamma) \rightarrow \mathcal{P}_0(\mathcal{T})$  the  $L^2$ -projection onto  $\mathcal{P}_0(\mathcal{T})$ , there holds for any  $u \in H^1(\Gamma_j)$

$$\|(\mathbb{1} - \Pi)u\|_{L^2(\Gamma_j)} = \inf_{v_h \in \mathcal{S}} \|u - v_h\|_{L^2(\Gamma_j)} \leq \inf_{v_h \in \mathcal{P}_0(\mathcal{T})} \|u - v_h\|_{L^2(\Gamma_j)} = \|(\mathbb{1} - \Pi_0)u\|_{L^2(\Gamma_j)}.$$

An application of the Poincaré inequality proves  $\|(\mathbb{1} - \Pi_0)u\|_{L^2(\Gamma_j)} \leq C_6 h_j \|\nabla u\|_{L^2(\Gamma_j)}$  with  $C_6 = 1/\pi$ . Hence, the operator  $T_\alpha : H^\alpha(\Gamma_j) \rightarrow L^2(\Gamma_j), u \mapsto u - \Pi_0 u$  has operator norm  $\|T_0\| = 1$  and  $\|T_1\| \leq C_6 h_j$  for  $\alpha = 0, 1$ , respectively. With the interpolation estimate (2.5), we infer  $\|T_\alpha\| \leq C_6^\alpha h_j^\alpha$  and therefore

$$(4.8) \quad \|(\mathbb{1} - \Pi)u\|_{L^2(\Gamma_j)} \leq C_6^\alpha h_j^\alpha \|u\|_{H^\alpha(\Gamma_j)}, \quad \text{for } u \in H^\alpha(\Gamma_j).$$

Now, let  $v \in L^2(\Gamma)$  and  $u \in H^\alpha(\Gamma)$ . The symmetry of orthogonal projections yields

$$(4.9) \quad \langle (\mathbb{1} - \Pi)v; u \rangle = \langle v; (\mathbb{1} - \Pi)u \rangle \leq \sum_{j=1}^n \|v\|_{L^2(\Gamma_j)} \|(\mathbb{1} - \Pi)u\|_{L^2(\Gamma_j)}.$$

The combination of (4.8)-(4.9) with Lemma 2.1 concludes the proof,

$$\langle (\mathbb{1} - \Pi)v; u \rangle \leq C_6^\alpha \sum_{j=1}^n \|h^\alpha v\|_{L^2(\Gamma_j)} \|u\|_{H^\alpha(\Gamma_j)} \leq C_6^\alpha \|h^\alpha v\|_{L^2(\Gamma)} \|u\|_{H^\alpha(\Gamma)}. \quad \square$$

**COROLLARY 4.2.** *For  $\alpha = 1/2$  and provided the assumptions of Theorem 4.1, the Galerkin projection  $\mathbb{G} : \tilde{H}^{-1/2}(\Gamma) \rightarrow \mathcal{S}$  onto  $\mathcal{S}$  has the local first-order approximation property.*

*Proof.* With the best approximation property  $\|(\mathbb{1} - \mathbb{G})v\| \leq \|(\mathbb{1} - \Pi)v\|$ , for all  $v \in L^2(\Gamma)$ , the proof follows from the equivalence of  $\|\cdot\|$  and the  $\tilde{H}^{-1/2}(\Gamma)$ -norm.  $\square$

The following elementary lemma sharpens the local first-order approximation property. It will be applied for  $\Pi$  and  $\mathbb{G}$  to obtain reliability of  $\mu_A$  and  $\mu_M$ , respectively.

**LEMMA 4.3.** *Let  $\mathcal{A} : L^2(\Gamma) \rightarrow \mathcal{P}_p(\mathcal{T})$  be idempotent [i.e.,  $\mathcal{A}^2 = \mathcal{A}$ ] and let  $\mathcal{A}$  satisfy (4.1). Then there holds for all  $v \in L^2(\Gamma)$ ,*

$$(4.10) \quad \|(\mathbb{1} - \mathcal{A})v\|_{\tilde{H}^{-\alpha}(\Gamma)} \leq C_{\text{apx}} \min \{ \|h^\alpha v\|_{L^2(\Gamma)}, \|h^\alpha (\mathbb{1} - \mathcal{A})v\|_{L^2(\Gamma)} \}.$$

*Proof.* Since  $(\mathbb{1} - \mathcal{A})$  is idempotent, we obtain from (4.1) for  $w := (\mathbb{1} - \mathcal{A})v \in L^2(\Gamma)$

$$\|w\|_{\tilde{H}^{-\alpha}(\Gamma)} = \|(\mathbb{1} - \mathcal{A})v\|_{\tilde{H}^{-\alpha}(\Gamma)} = \|(\mathbb{1} - \mathcal{A})w\|_{\tilde{H}^{-\alpha}(\Gamma)} \leq C_{\text{apx}} \|h^\alpha w\|_{L^2(\Gamma)}. \quad \square$$

**5. A posteriori error control by averaging techniques.** This section aims to provide a new class of error estimators and states their reliability and efficiency of which. We need two discrete finite element spaces  $\mathcal{S}_h$  and  $\mathcal{S}_H$ , where  $\mathcal{S}_h$  belongs to a finer mesh  $\mathcal{T}_h$  but lower polynomial degree as compared to  $\mathcal{S}_H$ .

**5.1. Assumptions and notations.** Fix two regular triangulations  $\mathcal{T}_h = \{\Gamma_1, \dots, \Gamma_n\}$  and  $\mathcal{T}_H = \{\gamma_1, \dots, \gamma_N\}$  with mesh sizes  $h \ll H$  [cf. (5.4) for a precise statement]. For integers  $0 \leq p < q$ , let  $\mathcal{S}_h$  and  $\mathcal{S}_H$  be subspaces of  $\mathcal{P}_p(\mathcal{T}_h)$  and  $\mathcal{P}_q(\mathcal{T}_H)$ , respectively. With respect to Theorem 4.1 we suppose that  $\mathcal{S}_h$  contains  $\mathcal{P}_0(\mathcal{T}_h)$  or  $\mathcal{P}_1(\mathcal{T}_h) \cap \mathcal{C}(\Gamma)$ .

Let  $u \in \tilde{H}^{-1/2}(\Gamma)$  denote the unique solution of (1.1), and let  $u_h \in \mathcal{S}_h$  be its Galerkin approximation with respect to  $\mathcal{S} = \mathcal{S}_h$  in (3.1). The Galerkin projection

$$(5.1) \quad \mathbb{G}_H : \tilde{H}^{-1/2}(\Gamma) \rightarrow \mathcal{S}_H \subseteq \tilde{H}^{-1/2}(\Gamma)$$

onto  $\mathcal{S}_H$  [i.e., the orthogonal projection onto  $\mathcal{S}_H$  with respect to the energy norm] is compared with an *arbitrary* [not necessarily linear or continuous] operator

$$(5.2) \quad \mathcal{A}_H : L^2(\Gamma) \rightarrow \mathcal{S}_H.$$

We consider the following four error estimators:

$$(5.3) \quad \begin{aligned} \eta_M &:= \|(\mathbb{1} - \mathbb{G}_H)u_h\|, & \mu_M &:= \|H^{1/2}(\mathbb{1} - \mathbb{G}_H)u_h\|_{L^2(\Gamma)}, \\ \eta_A &:= \|(\mathbb{1} - \mathcal{A}_H)u_h\|, & \mu_A &:= \|H^{1/2}(\mathbb{1} - \mathcal{A}_H)u_h\|_{L^2(\Gamma)}, \end{aligned}$$

i.e., we estimate the difference of the (low-order) discrete solution  $u_h$  on a finer mesh  $\mathcal{T}_h$  and a higher-order approximation of which on a coarser mesh  $\mathcal{T}_H$ .

In what follows, we use the inverse estimate (3.2) for [subspaces of]  $\mathcal{P}_p(\mathcal{T}_h)$ ,  $\mathcal{P}_q(\mathcal{T}_h)$ , and  $\mathcal{P}_q(\mathcal{T}_H)$ . To be precise, we therefore write, for instance,  $C_{\text{inv}}^{h,p} = C_{\text{inv}}(\Gamma, p, \mathcal{T}_h)$ . The analogous notation is used for the first-order approximation property of the  $L^2$ -projection [resp., Galerkin-projection] and we write, for instance,  $C_{\text{apx}}^{h,p}$ . Let  $\Pi_h : L^2(\Gamma) \rightarrow \mathcal{S}_h$  denote the  $L^2$ -projection onto  $\mathcal{S}_h$ , and let  $C_{\text{apx}}^{h,p} > 0$  be defined as in Theorem 4.1 with  $\mathcal{S} = \mathcal{S}_h$ . With the constant  $C_{\text{inv}}^{H,q} > 0$  in the inverse estimate (3.2) for  $\mathcal{S}_H$ , we assume

$$(5.4) \quad C_{\text{apx}}^{h,p} C_{\text{inv}}^{H,q} \max_{\gamma_j \in \mathcal{T}_H} (\|h\|_{L^\infty(\gamma_j)} / H_j)^{1/2} =: L < 1.$$

The analysis in the subsequent sections requires some additional regularity assumption on the exact solution, namely

$$(5.5) \quad u \in H^m(\mathcal{T}_H) \quad \text{for some } m > p + 1.$$

*Remark 5.1.* (i) The authors are aware that Assumption (5.5) is not reasonable for arbitrary Lipschitz screens  $\Gamma$  but requires some further (piecewise) smoothness of  $\Gamma$  so that  $H^m(\mathcal{T}_H)$  is well defined [SaS].

(ii) Even for slit problems [HMS] with smooth right-hand side  $f$  in (1.1), the solution  $u$  does not satisfy (5.5).

**5.2. The results.** The main theorem in section 5.3 states the reliability and efficiency of  $\eta_M$  [up to terms of higher order]. The perhaps surprising result is that  $\eta_A$  is always reliable; cf. Corollary 5.3. The explicit estimator  $\mu_A$  appears to be less costly compared with the other three since these involve the (approximate) computation of large full matrices; cf. section 8. The  $L^2$ -norm based estimators  $\mu_M$  and  $\mu_A$  immediately allow for local error indication for adaptive mesh-refining algorithms. Under weak additional assumptions [cf. section 5.4], we prove that  $\eta_M$  and  $\mu_M$ , respectively,  $\eta_A$  and  $\mu_A$  are equivalent, i.e., there are constants  $C_7, C_8 > 0$  such that there holds

$$C_7 \mu_M \leq \eta_M \leq C_8 \mu_M \quad \text{and} \quad C_7 \mu_A \leq \eta_A \leq C_8 \mu_A.$$

In the case that  $\mathcal{A}_H$  is the  $L^2$ -projection onto  $\mathcal{S}_H$  and provided that  $\mathcal{A}_H$  is  $H^1$ -stable, Theorem 5.6 states the efficiency of  $\eta_A$  and, in particular, of  $\mu_A$ .

**5.3. Reliability and efficiency of the error estimator  $\eta_M$ .** The idea of the following argument goes back at least to an Oberwolfach conference in the eighties as the authors learned from L.B. Wahlbin, but it has not been applied to integral equations before.

**THEOREM 5.1.** *Provided (5.4), there holds*

$$(5.6) \quad \|u - u_h\| \leq \frac{1}{1 - L} \|(\mathbf{1} - \mathbb{G}_H)(u - u_h)\|.$$

*Proof.* Define  $\tilde{h} \in \mathcal{P}_0(\mathcal{T}_H)$  by  $\tilde{h}|_{\gamma_j} := \|h\|_{L^\infty(\gamma_j)}$  for each element  $\gamma_j \in \mathcal{T}_H$ . For the Galerkin error  $e := u - u_h$ , the approximation property of  $\Pi_h$  yields

$$\|(\mathbf{1} - \Pi_h)\mathbb{G}_H e\| \leq C_{\text{apx}}^{h,p} \|h^{1/2} \mathbb{G}_H e\|_{L^2(\Gamma)} \leq C_{\text{apx}}^{h,p} \|\tilde{h}^{1/2} \mathbb{G}_H e\|_{L^2(\Gamma)}.$$

Now, we use the inverse estimate (3.2) for  $H^{1/2}\mathbb{G}_He \in \mathcal{P}_q(\mathcal{T}_H)$  and infer

$$\|\tilde{h}^{1/2}\mathbb{G}_He\|_{L^2(\Gamma)} \leq \|(\tilde{h}/H)^{1/2}\|_{L^\infty(\Gamma)} \|H^{1/2}\mathbb{G}_He\|_{L^2(\Gamma)} \leq C_{\text{inv}}^{H,q} \|(\tilde{h}/H)^{1/2}\|_{L^\infty(\Gamma)} \|\mathbb{G}_He\|.$$

The combination with the best approximation property  $\|\mathbb{G}_He\| \leq \|e\|$  shows

$$\|(\mathbf{1} - \Pi_h)\mathbb{G}_He\| \leq L\|e\|.$$

Using the Galerkin orthogonality and a Cauchy inequality, we obtain for  $\Pi_h\mathbb{G}_He \in \mathcal{S}_h$

$$\langle e; \mathbb{G}_He \rangle = \langle e; \mathbb{G}_He - \Pi_h\mathbb{G}_He \rangle \leq \|e\| \|(\mathbf{1} - \Pi_h)\mathbb{G}_He\| \leq L\|e\|^2.$$

Now, another Cauchy inequality leads to

$$\|e\|^2 = \langle e; \mathbb{G}_He \rangle + \langle e; e - \mathbb{G}_He \rangle \leq \|e\| (L\|e\| + \|(\mathbf{1} - \mathbb{G}_H)e\|).$$

This concludes the proof.  $\square$

*Remark 5.2.* The proof of Theorem 5.1 relies solely on the existence of an approximation operator  $P_h : L^2(\Gamma) \rightarrow \mathcal{S}_h$  with  $\|(\mathbf{1} - P_h)v_H\| \leq C_{\text{apx}} \|h^{1/2}v_H\|_{L^2(\Gamma)}$  for all  $v_H \in \mathcal{S}_H$ . If  $\Pi_h$  is replaced by such an operator  $P_h$ , the richness assumption on  $\mathcal{S}_h$  could be dropped.

*Remark 5.3.* Under the additional assumption  $u \in L^2(\Gamma)$ ,  $\mathbb{G}_H$  in Theorem 5.1 may be replaced by  $\mathcal{A}_H$  since the proof only needs that  $\mathcal{A}_H(u - u_h)$  is well defined. No further properties of  $\mathbb{G}_H$  enter.

*Remark 5.4.* In contrast to residual-based techniques, we could not derive analogous results for collocation or qualocation schemes since the proof of Theorem 5.1 makes explicit use of the Galerkin orthogonality.

**THEOREM 5.2.** *Provided (5.4) and (5.5), the error estimator  $\eta_M$  is reliable up to terms of higher order in the sense that*

$$(5.7) \quad \|u - u_h\| \leq \frac{1}{1-L} (\eta_M + \|(\mathbf{1} - \mathbb{G}_H)u\|)$$

with the constant  $0 < L < 1$  from Theorem 5.1, and also efficient up to terms of higher order, i.e.,

$$(5.8) \quad \eta_M \leq \|u - u_h\| + \|(\mathbf{1} - \mathbb{G}_H)u\|.$$

[Compared with  $\|u - u_h\|$  and  $\eta_M$ , the term  $\|(\mathbf{1} - \mathbb{G}_H)u\|$  is generically of higher order.]

*Proof.* According to (3.4), the error in the energy norm is of order

$$\|u - u_h\| = O(h_{\text{max}}^{\hat{p}}) \quad \text{with} \quad \hat{p} := \min\{p + 1, m\} + 1/2 = p + 3/2.$$

Furthermore, for smooth  $u$  we have

$$\|(\mathbf{1} - \mathbb{G}_H)u\| = O(H_{\text{max}}^{\hat{q}}) \quad \text{with} \quad \hat{q} := \min\{q + 1, m\} + 1/2 \geq \min\{p + 2, m\} + 1/2.$$

Since  $m > p + 1$ ,  $\|(\mathbf{1} - \mathbb{G}_H)u\|$  is of higher order. Theorem 5.1 combined with a triangle inequality shows

$$\|u - u_h\| \leq \frac{1}{1-L} (\|(\mathbf{1} - \mathbb{G}_H)u\| + \|(\mathbf{1} - \mathbb{G}_H)u_h\|)$$

and proves the reliability. A simple triangle inequality shows the efficiency

$$\eta_M \leq \|(\mathbf{1} - \mathbb{G}_H)(u - u_h)\| + \|(\mathbf{1} - \mathbb{G}_H)u\|,$$

since  $(\mathbf{1} - \mathbb{G}_H)$  is an orthogonal projection with respect to the energy norm.  $\square$

**5.4. Reliability of the error estimators  $\eta_A$ ,  $\mu_A$ , and  $\mu_M$ .** Replacing the best approximation operator  $\mathbb{G}_H$  by another operator  $\mathcal{A}_H$ , we immediately obtain the following corollary.

COROLLARY 5.3. *We always have  $\eta_M \leq \eta_A$ , i.e., (5.4), (5.5) the error estimator  $\eta_A$  is reliable up to terms of higher order.  $\square$*

This and an application of Lemma 4.3 proves the reliability of  $\mu_A$  and  $\mu_M$ .

COROLLARY 5.4. *Suppose that  $\mathcal{A}_H : L^2(\Gamma) \rightarrow \mathcal{S}_H \subseteq L^2(\Gamma)$  is a projection having the local first-order approximation property (4.1) with respect to the energy norm. Then,*

$$(5.9) \quad \eta_A \leq C_{\text{apx}}^{H,q} \mu_A.$$

*In particular,  $\mu_M$  is reliable up to terms of higher order provided (5.4), (5.5) and, additionally,  $\mathcal{P}_0(\mathcal{T}_H) \subseteq \mathcal{S}_H$  or  $\mathcal{P}_1(\mathcal{T}_H) \cap \mathcal{C}(\Gamma) \subseteq \mathcal{S}_H$ .  $\square$*

An application of the inverse estimate (3.2) shows that  $\mu_A$  is efficient if and only if  $\eta_A$  is efficient.

COROLLARY 5.5. *Let  $C_9 := \max_{\Gamma_j \in \mathcal{T}_h} (\|H\|_{L^\infty(\Gamma_j)} / h_j)^{1/2}$ . Provided  $\mathcal{S}_H \subseteq \mathcal{P}_q(\mathcal{T}_h)$  there holds*

$$(5.10) \quad \mu_A \leq C_9 C_{\text{inv}}^{h,q} \eta_A.$$

*In particular,  $\mu_M$  is efficient up to terms of higher order.  $\square$*

Remark 5.5. Note that the assumption  $\mathcal{S}_H \subseteq \mathcal{P}_q(\mathcal{T}_h)$  is quite weak and, in particular, satisfied if  $\mathcal{T}_h$  is obtained by refinements of  $\mathcal{T}_H$ .

**5.5. Efficiency of  $\eta_A$  and  $\mu_A$  for the  $L^2$ -projection.** For the remaining part of this section, we suppose that the interpolation operator  $\mathcal{A}_H = \Pi_H$  is just the  $L^2$ -projection onto  $\mathcal{S}_H \subseteq H^1(\Gamma)$ .

DEFINITION 2. *The  $L^2$ -projection  $\mathcal{A}_H : L^2(\Gamma) \rightarrow \mathcal{S}_H$  onto  $\mathcal{S}_H$  is called  $H^1$ -stable if there holds*

$$(5.11) \quad \|\mathcal{A}_H v\|_{H^1(\Gamma)} \leq C_{10} \|v\|_{H^1(\Gamma)} \quad \text{for all } v \in H^1(\Gamma),$$

where the constant  $C_{10} > 0$  depends only on  $\Gamma, q$ , and the shape of the elements in  $\mathcal{T}_H$  but not on their number or size.

THEOREM 5.6. *Provided (5.4), (5.5) and  $H^1$ -stability of the  $L^2$ -projection  $\mathcal{A}_H : L^2(\Gamma) \rightarrow \mathcal{S}_H$  onto  $\mathcal{S}_H$ , the error estimator  $\eta_A$  is reliable and efficient up to terms of higher order.*

*Proof.* Define the operator  $T_\alpha = (\mathbf{1} - \mathcal{A}_H) : H^\alpha(\Gamma) \rightarrow H^\alpha(\Gamma)$  which is linear and continuous for  $\alpha = 0$  and  $\alpha = 1$ , respectively. Interpolation yields continuity of  $T_{1/2}$  with operator norm  $\|T_{1/2}\| \leq \|T_1\|^{1/2}$  since  $\|T_0\| = 1$ . We consider the adjoint operator  $T_{1/2}^* : \tilde{H}^{-1/2}(\Gamma) \rightarrow \tilde{H}^{-1/2}(\Gamma)$  defined formally by

$$(5.12) \quad \langle T_{1/2}^* w; v \rangle = \langle w; T_{1/2} v \rangle \quad \text{for } w \in \tilde{H}^{-1/2}(\Gamma), v \in H^{1/2}(\Gamma).$$

Notice that, for  $w \in L^2(\Gamma)$ , we have  $T_{1/2}^* w = T_{1/2} w$  according to the symmetry of the orthogonal projection  $T_0$  and the  $L^2$  scalar product on the right-hand side of (5.12) in case  $w \in L^2(\Gamma)$ . Since  $T_{1/2}^*$  is continuous, let  $C_{11} < \infty$  denote the operator norm of  $T_{1/2}^*$  with respect to the energy norm. As above, a simple triangle inequality shows

$$(5.13) \quad \eta_A \leq \|(\mathbf{1} - \mathcal{A}_H)(u - u_h)\| + \|(\mathbf{1} - \mathcal{A}_H)u\| \leq C_{11} \|u - u_h\| + \|(\mathbf{1} - \mathcal{A}_H)u\|,$$

where we have used  $u - u_h \in L^2(\Gamma)$  and  $T_{1/2}^*(u - u_h) = (\mathbb{1} - \mathcal{A}_H)(u - u_h)$ . Theorem 4.1 and a standard approximation result in  $L^2$  yield

$$\|(\mathbb{1} - \mathcal{A}_H)u\| \leq C_{\text{apx}} H_{\text{max}}^{1/2} \|(\mathbb{1} - \mathcal{A}_H)u\|_{L^2(\Gamma)} = O(H_{\text{max}}^{\hat{q}+1/2}) \quad \text{with} \quad \hat{q} := \min\{q + 1, m\}.$$

Therefore, the last term in (5.13) is of higher order; cf. the proof of Theorem 5.2.  $\square$

The efficiency of  $\mu_A$  follows from the previous section.

**COROLLARY 5.7.** *Provided  $\mathcal{P}_1(\mathcal{T}_H) \cap \mathcal{C}(\Gamma) \subseteq \mathcal{S}_H \subseteq \mathcal{P}_q(\mathcal{T}_h)$ , there holds*

$$(5.14) \quad \mu_A \leq C_9 C_{\text{inv}}^{h,q} \eta_A \quad \text{and} \quad \eta_A \leq C_{\text{apx}}^{H,q} \mu_A,$$

whence the error estimator  $\mu_A$  is reliable and efficient up to terms of higher order under the assumptions of Theorem 5.6.  $\square$

*Remark 5.6.* For special cases it is easy to derive the efficiency of  $\eta_A$  although  $\mathcal{S}_H \not\subseteq H^1(\Gamma)$ . For instance, assume  $\mathcal{S}_h = \mathcal{P}_0(\mathcal{T}_h)$  and  $\mathcal{S}_H = \mathcal{P}_1(\mathcal{T}_H) \subseteq \mathcal{P}_1(\mathcal{T}_h)$ . Suppose that  $\mathcal{A}_H$  is the  $L^2$ -projection onto  $\mathcal{S}_H$  and  $\Pi_H$  is the  $L^2$ -projection onto  $\mathcal{P}_1(\mathcal{T}_H) \cap \mathcal{C}(\Gamma)$ . An application of the derived results shows

$$\eta_A \lesssim \|H^{1/2}(\mathbb{1} - \mathcal{A}_H)u_h\|_{L^2(\Gamma)} \leq \|H^{1/2}(\mathbb{1} - \Pi_H)u_h\|_{L^2(\Gamma)} \lesssim \|u - u_h\|,$$

where  $\lesssim$  denotes  $\leq$  up to a mesh size independent constant.

**6. Numerical realization in two dimensions.** For the numerical experiments, we choose  $\mathcal{S}_h = \mathcal{P}_0(\mathcal{T}_h)$  and  $\mathcal{S}_H = \mathcal{P}_1(\mathcal{T}_H)$ . The finer mesh  $\mathcal{T}_h$  is obtained from the coarser  $\mathcal{T}_H$  by uniform refinements; cf. section 6.3 for details. This ensures  $\mathcal{S}_H = \mathcal{P}_1(\mathcal{T}_H) \subseteq \mathcal{P}_1(\mathcal{T}_h)$ . The approximation  $u_h \in \mathcal{S}_h$  is then defined by  $u_h|_{\Gamma_j} = \mathbf{x}_j$ , where  $\mathbf{x} \in \mathbb{R}^n$  is the solution of a linear system

$$(6.1) \quad \mathbf{Ax} = \mathbf{b}.$$

In all numerical experiments we consider the error estimators  $\eta_M, \mu_M$  based on the Galerkin projection  $\mathbb{G}_H$  and the error estimators  $\eta_A, \mu_A$  based on the  $L^2$ -projection  $\mathcal{A}_H = \Pi_H$ .

**6.1. Poisson problem and Symm's integral equation.** In the numerical experiments we consider three examples where the right-hand side  $f$  in (1.1) comes from a Poisson problem

$$(6.2) \quad \Delta U = 0 \text{ in } \Omega \quad \text{and} \quad U = g \text{ on } \Gamma = \partial\Omega$$

with given Dirichlet data  $g$  on  $\Gamma$  [plus boundary conditions at infinity if  $\Omega$  is unbounded]. This problem is equivalent to Symm's integral equation (1.1), where  $f$  takes the form  $f = (K + \mathbb{1})g$  with the double-layer potential operator  $K$ , defined as Cauchy principal value by

$$(6.3) \quad (Kg)(x) := -\frac{1}{\pi} \oint_{\Gamma} g(y) \frac{(y-x) \cdot n(y)}{|x-y|^2} ds_y \quad \text{for } x \in \Gamma.$$

Then, the exact solution of (1.1) is just the normal derivative  $u = \partial U / \partial n$  of  $U$  on the boundary  $\Gamma$ . Notice that  $Kg$  vanishes on  $\Gamma$  whenever  $\Gamma$  is a slit.

**6.2. Computation of the discrete solution.** The coefficients of the stiffness matrix  $\mathbf{A} \in \mathbb{R}_{sym}^{n \times n}$  are computed by

$$(6.4) \quad \mathbf{A}_{jk} := \langle \chi_j; \chi_k \rangle = -\frac{1}{\pi} \int_{\Gamma_j} \int_{\Gamma_k} \log |x - y| ds_y ds_x.$$

Here,  $\chi_j$  denotes the characteristic function of the set  $\Gamma_j \subseteq \mathbb{R}^2$  [i.e.,  $\chi_j(x) = 1$  if  $x \in \Gamma_j$  and  $\chi_j(x) = 0$  else]. The right-hand side  $\mathbf{b} \in \mathbb{R}^n$  is given by

$$(6.5) \quad \mathbf{b}_j := \int_{\Gamma_j} f(x) ds_x$$

with  $f$  from (1.1). While  $\mathbf{A}_{jk}$  can be computed analytically [Ma], the computation of  $\mathbf{b}_j$  involves proper quadrature rules—in particular, if the right-hand side is induced by a Poisson problem; cf. [CP1, section 6].

**6.3. Adaptive algorithm.** All mesh refinements are performed with the following adaptive algorithm based on the refinement indicators  $\mu_{M,j}$  or  $\mu_{A,j}$  defined as follows: Given the coarse mesh  $\mathcal{T}_H = \{\gamma_1, \dots, \gamma_N\}$  and the  $L^2$ -projection  $\Pi_H : \mathcal{P}_0(\mathcal{T}_h) \rightarrow \mathcal{P}_1(\mathcal{T}_H)$ , we define

$$(6.6) \quad \mu_{M,j} := H_j^{1/2} \|(\mathbb{1} - \mathbb{G}_H)u_h\|_{L^2(\gamma_j)}, \quad \text{respectively,} \quad \mu_{A,j} := H_j^{1/2} \|(\mathbb{1} - \Pi_H)u_h\|_{L^2(\gamma_j)}$$

for  $j = 1, \dots, N$ ,

i.e.,  $\mu_M = (\sum_{j=1}^N \mu_{M,j}^2)^{1/2}$  and  $\mu_A = (\sum_{j=1}^N \mu_{A,j}^2)^{1/2}$ , respectively.

ALGORITHM 6.1. Choose an initial mesh  $\mathcal{T}_H^{(0)}$ ,  $k = 0$ ,  $\ell \in \mathbb{N}_{\geq 2}$ , and  $0 \leq \theta \leq 1$ .

- (i) Obtain  $\mathcal{T}_h^{(k)} = \{\Gamma_1, \dots, \Gamma_n\}$  from  $\mathcal{T}_H^{(k)} = \{\gamma_1, \dots, \gamma_N\}$  by uniform splitting of each element  $\gamma_j \in \mathcal{T}_H^{(k)}$  into  $\ell$  elements of equal length.
- (ii) Compute the approximation  $u_h^{(k)}$  for the current mesh  $\mathcal{T}_h^{(k)}$ .
- (iii) Compute error estimators  $\eta_M$  and  $\eta_A$  and refinement indicators  $\mu_{M,j}$  and  $\mu_{A,j}$ .
- (iv) Mark element  $\gamma_j$  provided the corresponding refinement estimator satisfies  $\mu_{M,j} \geq \theta \max\{\mu_{M,1}, \dots, \mu_{M,N}\}$  and  $\mu_{A,j} \geq \theta \max\{\mu_{A,1}, \dots, \mu_{A,N}\}$ , respectively.
- (v) Halve all marked elements  $\gamma_j \in \mathcal{T}_H^{(k)}$  and so generate a new coarse mesh  $\mathcal{T}_H^{(k+1)}$ , update  $k$ , and go to (i).

**7. Numerical experiments in two dimensions.** This section reports on some numerical experiments to study the accuracy of the introduced error estimators and the performance of the proposed adaptive strategy. All computations are done with MATLAB. Example 7.1 corresponds to a Dirichlet problem with smooth solution such that the smoothness assumptions in section 5 are satisfied and guarantee reliability and efficiency of our error estimators. Examples 7.2–7.4 are taken from [CP1] and [ChS], respectively. They have been realized and studied in [CP1] for adaptive mesh-refinement with respect to the residual-based error estimator introduced by Faermann [F1, F2, F3]; cf. (7.3). Example 7.2 considers Symm's integral equation corresponding to a Dirichlet problem on the L-shaped domain. The exact solution is known and has a singularity at the reentrant corner. Therefore, adaptivity is necessary to retain the optimal convergence rate. Example 7.3 deals with a constant

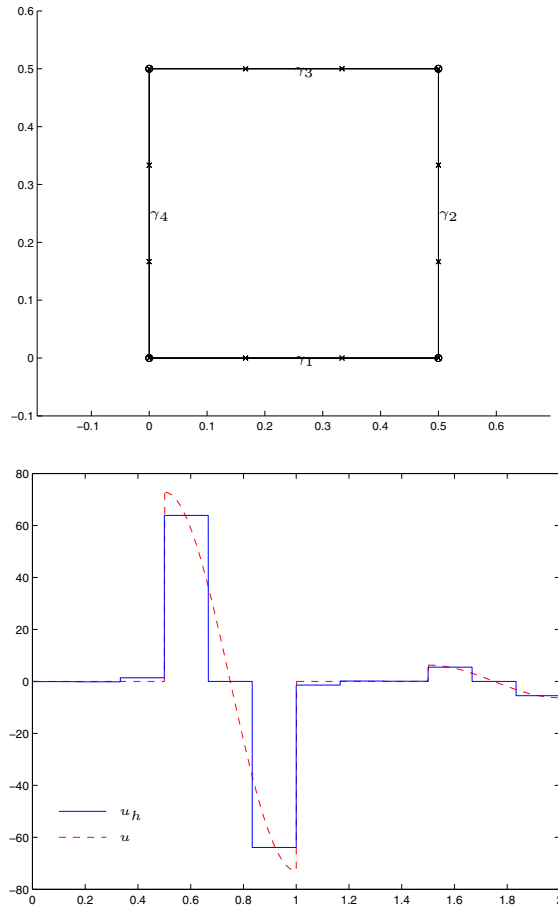


FIG. 1. Initial coarse mesh  $\mathcal{T}_H^{(0)}$  in Poisson problem 7.1 with  $N = 4$  elements [nodes indicated by  $\circ$ ] (top) and the corresponding refined mesh  $\mathcal{T}_h^{(0)}$  for  $\ell = 3$  in Algorithm 6.1, i.e.  $n = 12$  [nodes indicated by  $\times$ ]. The related discrete solution  $u_h$  on  $\mathcal{T}_h^{(0)}$  (bottom) is plotted over the arclength  $s = 0, \dots, 2$  of  $\Gamma$ . The exact solution  $u$  from (7.6) is shown for comparison (bottom);  $u$  is piecewise smooth and jumps together with the outer normal in the corners of  $\Gamma$  [for arclength parameters  $s = 1/2, 1, 3/2$ , and  $2$ ].

right-hand side to exclude positive and negative effects due to quadrature errors. The exact solution is unknown. The sequence of discrete solutions shows singularities at the five rectangular corners of the L-shape. Example 7.4 taken from [ChS] considers a slit problem, where the known exact solution  $u$  lacks almost any smoothness, more precisely  $u \notin L^2(\Gamma)$ . Finally, Example 7.5 involves the approximation of a smooth boundary by a polygonal boundary. We approximate a smooth eigenfunction of the single-layer potential on the sphere with radius  $1/2$ .

**Preliminaries.** Uniform and adaptive meshes as well as plots of discrete and exact solutions  $u_h$  and  $u$  are shown in Figures 1, 4, and 10 as functions of its arclength parametrization  $s$ ,  $0 \leq s \leq \text{length}(\Gamma) = 2$ . Furthermore, errors and estimators are considered for the energy norm. Various numbers are provided in Tables 1, 2, and 3 and even more convergence results are visualized in Figures 2, 5–7, 9, 11, 13, and

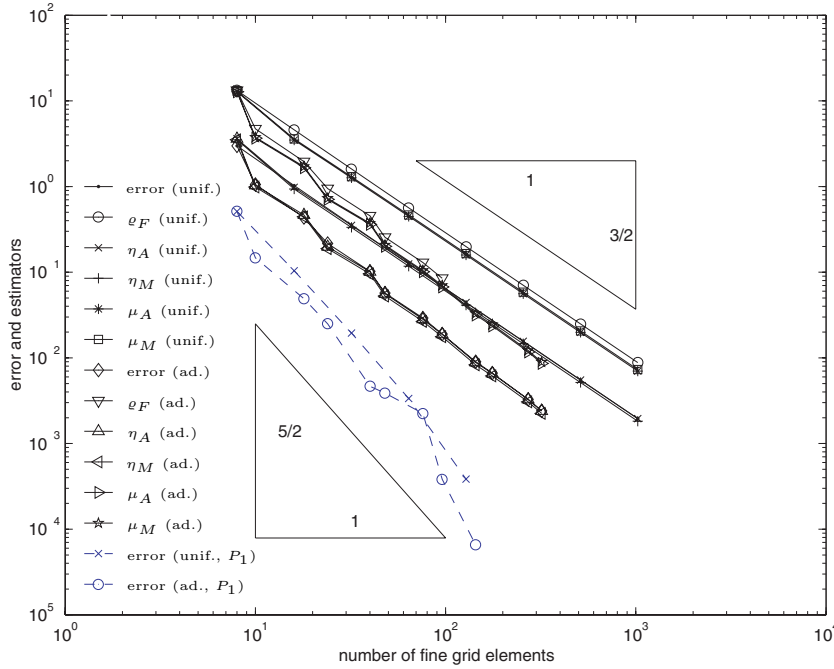


FIG. 2. Error and error estimators  $\eta_M$ ,  $\eta_A$ ,  $\mu_M$ , and  $\mu_A$  for uniform [indicated by unif.] and  $\mu_A$ -adaptive [indicated by ad.] mesh refinement in Poisson problem 7.1 and  $\ell = 2$  in Algorithm 6.1. The  $\mathcal{P}_0$  boundary element method leads to the optimal convergence rate  $h^{3/2}$ . For comparison, also the error for the  $\mathcal{P}_1$  boundary element method [dashed lines] on the generated meshes [i.e., uniform, resp.,  $\mu_A$ -adaptive] is shown. As expected, one again observes the optimal experimental convergence rate  $h^{5/2}$ .

16. Some adaptively generated meshes are shown in Figures 3, 12, and 14.

We compute the experimental convergence rate of the error

$$(7.1) \quad E^{(k)} := \|u - u_h^{(k)}\| = (\|u\|^2 - \|u_h^{(k)}\|^2)^{1/2}$$

by the formula

$$(7.2) \quad \kappa^{(k)} = \log(E^{(k-1)}/E^{(k)}) / \log(n^{(k)}/n^{(k-1)}).$$

Here,  $n^{(k)} = \text{card}(\mathcal{T}_h^{(k)})$  denotes the number of elements. The energy norm of the discrete solution  $u_h$  reads  $\|u_h\|^2 = \mathbf{x} \cdot \mathbf{A} \mathbf{x}$  with the stiffness matrix  $\mathbf{A}$  and the coefficient vector  $\mathbf{x}$  introduced in section 6. The energy norm  $\|u\|$  of the exact solution is either computed exactly or obtained by Aitkin's  $\Delta^2$  extrapolation of the sequence of values for discrete solutions on uniformly refined meshes.

For comparison, in Figures 2, 5–7, 11, 13, and 16 we also show the residual-based error estimator  $\varrho_F$  introduced by Faermann,

$$(7.3) \quad \varrho_F := \left( \sum_{j=1}^n \varrho_{F,j}^2 \right)^{1/2},$$

where the refinement indicators

TABLE 1

Experimental error, error estimator  $\eta_M$  and  $\eta_A$ , and convergence rates for Poisson problem 7.1,  $\ell = 2$ , and uniform (top), respectively,  $\mu_A$ -adaptive mesh refinement (bottom).

Uniform mesh refinement							
$k$	$n$	$E$	$\eta_M$	$\eta_A$	$\eta_M/E$	$\eta_M/\eta_A$	$\kappa$
0	8	2.9820e+00	3.5112e+00	3.6134e+00	1.18	0.97	
1	16	1.0276e+00	9.3703e-01	9.8030e-01	0.91	0.96	1.54
2	32	3.5630e-01	3.3380e-01	3.5308e-01	0.94	0.95	1.53
3	64	1.2519e-01	1.1730e-01	1.2496e-01	0.94	0.94	1.51
4	128	4.4187e-02	4.1356e-02	4.4168e-02	0.94	0.94	1.50
5	256	1.5615e-02	1.4609e-02	1.5614e-02	0.94	0.94	1.50
6	512	5.5202e-03	5.1640e-03	5.5201e-03	0.94	0.94	1.50
7	1024	1.9514e-03	1.8256e-03	1.9516e-03	0.94	0.94	1.50
Adaptive mesh refinement							
$k$	$n$	$E$	$\eta_M$	$\eta_A$	$\eta_M/E$	$\eta_M/\eta_A$	$\kappa$
0	8	2.9820e+00	3.5112e+00	3.6134e+00	1.18	0.97	
1	10	1.0570e+00	9.8846e-01	1.0292e+00	0.94	0.96	4.65
2	18	4.3445e-01	4.4375e-01	4.6590e-01	1.02	0.95	1.51
3	24	2.1601e-01	1.8876e-01	1.9815e-01	0.87	0.95	2.43
4	40	1.0226e-01	9.5542e-02	1.0109e-01	0.93	0.95	1.46
5	48	5.7202e-02	5.2676e-02	5.5940e-02	0.92	0.94	3.19
6	76	2.9243e-02	2.6660e-02	2.8243e-02	0.91	0.94	1.46
7	96	1.8958e-02	1.7670e-02	1.8807e-02	0.93	0.94	1.86
8	144	9.0153e-03	8.2982e-03	8.8322e-03	0.92	0.94	1.83
9	176	6.6515e-03	6.1626e-03	6.5680e-03	0.93	0.94	1.52
10	272	3.2840e-03	3.0642e-03	3.2651e-03	0.93	0.94	1.62

TABLE 2

Experimental error and error estimator  $\mu_M$ ,  $\mu_A$ , and  $\varrho_F$  for Poisson problem 7.1,  $\ell = 2$ , and uniform (top), respectively,  $\mu_A$ -adaptive mesh refinement (bottom).

Uniform mesh refinement									
$k$	$n$	$E$	$\mu_M$	$\mu_A$	$\varrho_F$	$\mu_M/E$	$\mu_A/E$	$\mu_M/\mu_A$	$\varrho_F/E$
0	8	2.982e+00	1.302e+01	1.278e+01	1.328e+01	4.37	4.29	1.02	4.45
1	16	1.028e+00	3.592e+00	3.496e+00	4.593e+00	3.50	3.40	1.03	4.47
2	32	3.563e-01	1.307e+00	1.264e+00	1.602e+00	3.67	3.55	1.03	4.50
3	64	1.252e-01	4.655e-01	4.484e-01	5.638e-01	3.72	3.58	1.04	4.50
4	128	4.419e-02	1.649e-01	1.586e-01	1.991e-01	3.73	3.59	1.04	4.51
5	256	1.562e-02	5.835e-02	5.607e-02	7.036e-02	3.74	3.59	1.04	4.51
6	512	5.520e-03	2.063e-02	1.982e-02	2.487e-02	3.74	3.59	1.04	4.51
7	1024	1.951e-03	7.295e-03	7.009e-03	8.794e-03	3.74	3.59	1.04	4.51
Adaptive mesh refinement									
$k$	$n$	$E$	$\mu_M$	$\mu_A$	$\varrho_F$	$\mu_M/E$	$\mu_A/E$	$\mu_M/\mu_A$	$\varrho_F/E$
0	8	2.982e+00	1.302e+01	1.278e+01	1.328e+01	4.37	4.29	1.02	4.45
1	10	1.057e+00	3.755e+00	3.667e+00	4.721e+00	3.55	3.47	1.02	4.47
2	18	4.344e-01	1.710e+00	1.660e+00	1.952e+00	3.94	3.82	1.03	4.49
3	24	2.160e-01	7.278e-01	7.072e-01	9.458e-01	3.37	3.27	1.03	4.38
4	40	1.023e-01	3.738e-01	3.616e-01	4.546e-01	3.66	3.54	1.03	4.45
5	48	5.720e-02	2.078e-01	2.005e-01	2.560e-01	3.63	3.51	1.04	4.47
6	76	2.924e-02	1.046e-01	1.011e-01	1.297e-01	3.58	3.46	1.03	4.43
7	96	1.896e-02	6.998e-02	6.742e-02	8.484e-02	3.69	3.56	1.04	4.48
8	144	9.015e-03	3.287e-02	3.167e-02	4.026e-02	3.65	3.51	1.04	4.47
9	176	6.651e-03	2.448e-02	2.356e-02	2.979e-02	3.68	3.54	1.04	4.48
10	272	3.284e-03	1.216e-02	1.171e-02	1.472e-02	3.70	3.57	1.04	4.48

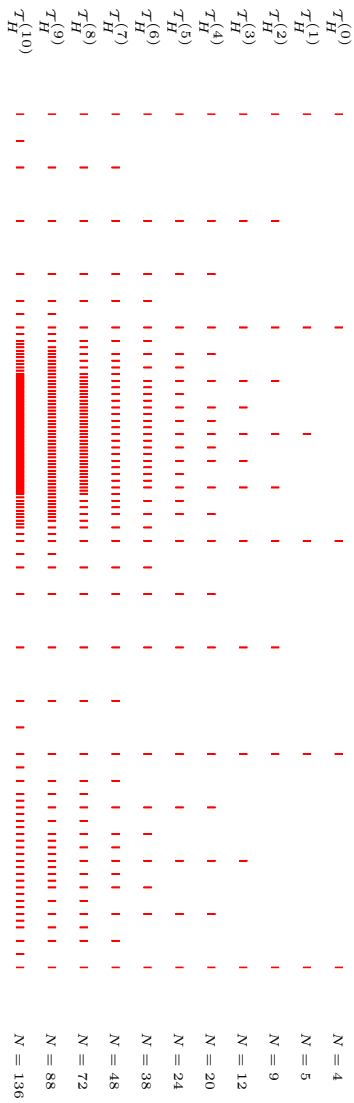


FIG. 3. Adaptive mesh refinement in Poisson problem T.1 related to  $\ell = 2$  and error estimator  $\mu_A$ . Adaptive mesh refinement with respect to  $\mu_V$  leads to the same meshes.

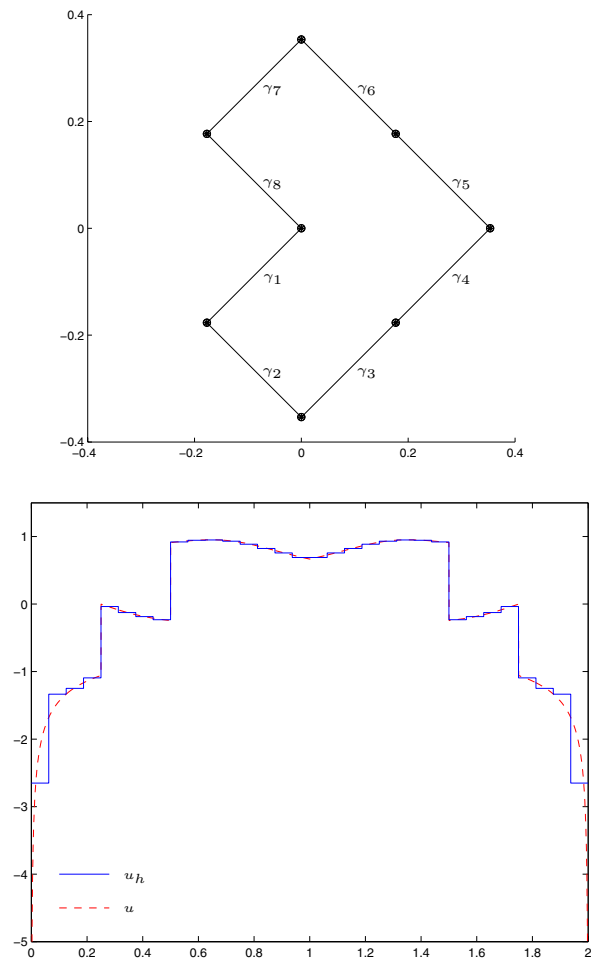


FIG. 4. Initial coarse mesh  $\mathcal{T}_H^{(0)}$  in Poisson problems 7.2 and 7.3 with  $N = 8$  elements (top) and the corresponding discrete solution  $u_h$  on  $\mathcal{T}_h^{(0)}$  for  $\ell = 4$ , i.e.,  $n = 32$  fine grid elements, in Poisson problem 7.2 (bottom). The exact solution  $u$  from (7.8) is shown for comparison (bottom).

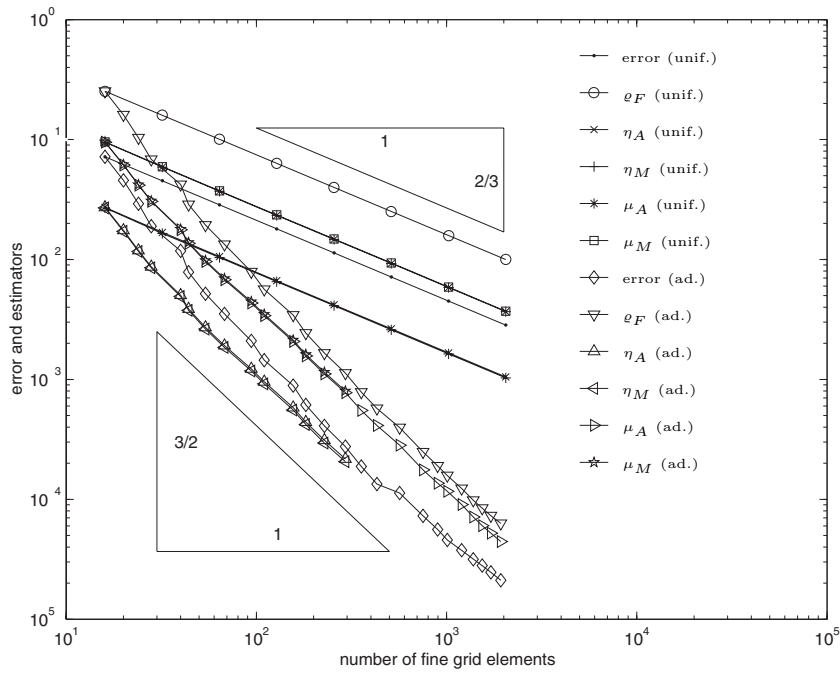


FIG. 5. Error and error estimators  $\eta_M$ ,  $\eta_A$ ,  $\mu_M$ , and  $\mu_A$  for uniform [indicated by unif.] and  $\mu_A$ -adaptive [indicated by ad.] mesh refinement in Poisson problem 7.2 and  $\ell = 2$  in Algorithm 6.1.

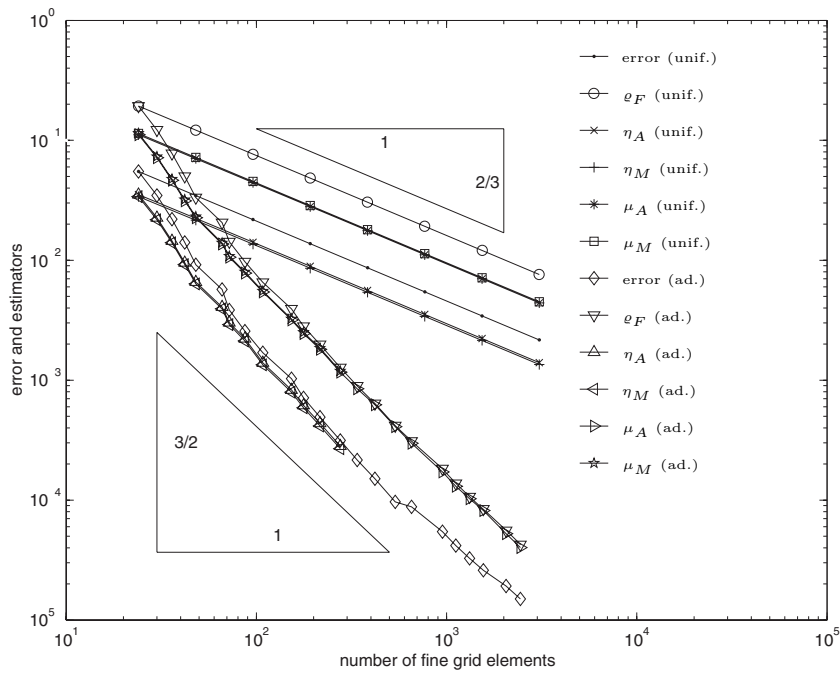


FIG. 6. Error and error estimators  $\eta_M$ ,  $\eta_A$ ,  $\mu_M$ , and  $\mu_A$  for uniform [indicated by unif.] and  $\mu_A$ -adaptive [indicated by ad.] mesh refinement in Poisson problem 7.2 and  $\ell = 3$  in Algorithm 6.1.

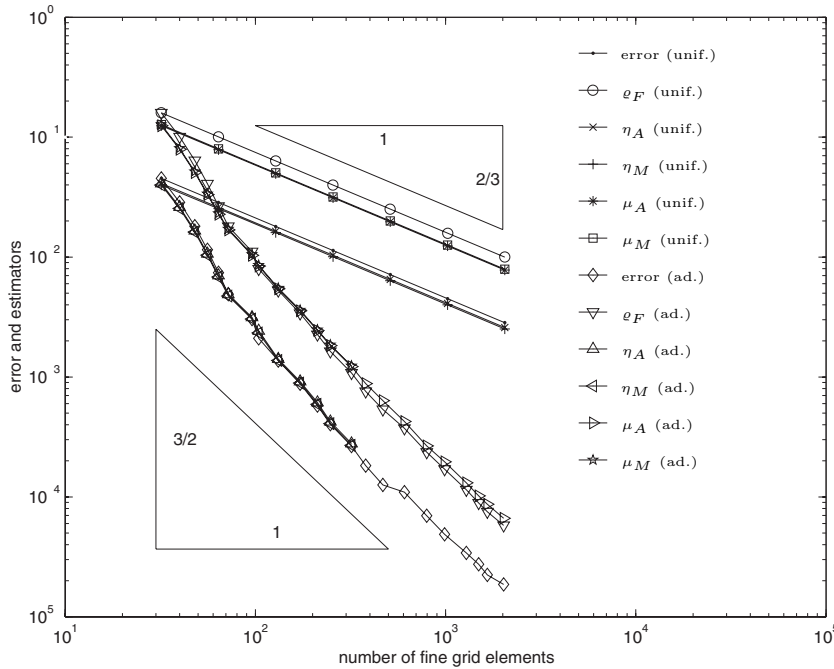


FIG. 7. Error and error estimators  $\eta_M$ ,  $\eta_A$ ,  $\mu_M$ , and  $\mu_A$  for uniform [indicated by unif.] and  $\mu_A$ -adaptive [indicated by ad.] mesh refinement in Poisson problem 7.2 and  $\ell = 4$  in Algorithm 6.1.

$$(7.4) \quad \varrho_{F,j} := \int_{\Gamma_j \cup \Gamma_{j+1}} \int_{\Gamma_j \cup \Gamma_{j+1}} \frac{|r_h(x) - r_h(y)|^2}{|x - y|^2} ds_y ds_x$$

are local Sobolev–Slobodeckij seminorms of the residual  $r_h := f - Vu_h \in H^{1/2}(\Gamma)$ . This estimator is known to be reliable and efficient for the Galerkin method. Details on the numerical realization of these double boundary integrals are provided in [CP1]. Since the reliability and efficiency of this estimator depends in 2D on the local mesh ratio

$$(7.5) \quad \kappa(\mathcal{T}_h) = \max\{h_{T_j}/h_{T_k} : T_j, T_k \in \mathcal{T}_h \text{ neighbors}\},$$

we extend the marking strategy in (iv) of Algorithm 6.1 to ensure that there holds  $\kappa(\mathcal{T}_H) \leq 2$ , i.e., that the mesh size of two neighboring coarse elements varies at most by 2.

**7.1. Poisson-problem with smooth solution.** We consider problem (6.2) on the halved unit square  $\Omega = [0, 1/2]^2$  with exact solution  $U(x, y) = \sinh(2\pi x) \cos(2\pi y)$  and solve the corresponding Symm’s integral equation  $Vu = f$  with right-hand side  $f = (K + 1)g$  and  $g = U|_\Gamma$ . Then,  $u = \partial U/\partial n$  is smooth on each affine boundary piece,

$$(7.6) \quad u(x, y) = 2\pi \begin{pmatrix} \cosh(2\pi x) \cos(2\pi y) \\ -\sinh(2\pi x) \sin(2\pi y) \end{pmatrix} \cdot n(x, y)$$

with the outer normal  $n(x, y)$  of  $\Omega$  on  $\Gamma = \partial\Omega$ , and we expect to obtain optimal convergence rate  $\mathcal{O}(n^{3/2})$  even for uniform mesh refinement. Notice that  $u$  vanishes on  $[0, 1/2] \times \{0, 1/2\}$ , i.e., on the lower and upper boundary of  $\Omega$ .

Figure 1 shows the initial coarse mesh  $\mathcal{T}_H^{(0)}$ , the exact solution  $u$  from (7.6) plotted over the arclength  $s = 0, \dots, 2$ , and a discrete solution  $u_h$  corresponding to  $\mathcal{T}_h^{(0)}$  with  $\ell = 3$  in Algorithm 6.1. As can be seen,  $u$  vanishes on the parameter intervals  $0 \leq s \leq 1/2$  and  $1 \leq s \leq 3/2$ . On the other two affine boundary pieces,  $u$  is smooth and jumps with the normal vector in the corners of  $\Gamma$ .

Figure 2 shows errors and error estimators for both uniform and  $\mu_A$ -adaptive mesh refinement and  $\ell = 2$  in Algorithm 6.1. All values are shown on a log-log scale so that the experimental convergence rates (7.2) of both the error and the estimators are visible as the slope of the corresponding curves. The error  $E = \|u - u_h\|$  is computed via (7.1), where the energy norm of the exact solution is obtained by extrapolation,  $\|u\|^2 = 162.1448097$ . As is to be expected from the regularity of  $u$ , uniform mesh refinement leads to the optimal experimental convergence rate  $h^{3/2}$ . The curve for the error on adaptively generated meshes is parallel, but the absolute values are improved by a factor of 5. This improvement can be explained by the fact that the adaptive algorithm mainly resolves the strong growth of the function within the arclength parameter intervals  $1/2 \leq s \leq 1$  and  $3/2 \leq s \leq 2$ , where  $u$  does not vanish; cf. Figure 1. The corresponding adaptive meshes are shown in Figure 3. For comparison, Figure 2 also shows the error for the  $\mathcal{P}_1$  boundary element methods on the same meshes, since this term corresponds to the higher-order terms of our error estimates. As expected, the  $\mathcal{P}_1$ -error shows the optimal experimental convergence rate of  $h^{5/2}$ .

For both  $\mathcal{P}_0$  and  $\mathcal{P}_1$  boundary element methods, the error shows no preasymptotic behavior but converges with optimal convergence order from the very start. This is reflected by the error estimation of the  $\mathcal{P}_0$  error  $E = \|u - u_h\|$  by the error estimators  $\eta_M$  and  $\eta_A$ . The error is very sharply estimated: The values of both estimators almost coincide with the corresponding error value. This is also underlined by several numbers in Table 1: The quotients  $\eta_M/E$ , respectively,  $\eta_M/\eta_A$  converge to approximately 0.94 and 0.93 for both uniform and adaptive mesh refinement. The performance of the  $L^2$ -error estimators  $\mu_M$  and  $\mu_A$  is examined in Table 2. The error estimator  $\mu_M$  and  $\mu_A$  almost coincide. The quotient  $\mu_M/\mu_A$  stays bounded by approximately 1.04. The error is overestimated by a factor 3.5–3.7. For comparison, note that the Faermann error estimator  $\varrho_F$  overestimates the error by a factor 4.4, 4.5.

**7.2. Poisson-problem on L-shaped domain.** For a fixed parameter  $\alpha > 0$  we consider Problem (6.2) on the L-shaped domain  $\Omega$  shown in Figure 4 with exact solution

$$(7.7) \quad U(x) = r^\alpha \cos(\alpha\varphi) \quad \text{in polar coordinates} \quad x = r(\cos\varphi, \sin\varphi).$$

Then, the exact solution  $u$  of Symm's integral equation reads in polar coordinates

$$(7.8) \quad u(x) = (w \cdot n(x)) \alpha r^{\alpha-1} \quad \text{with } w := \begin{pmatrix} \cos(\varphi) \cos(\alpha\varphi) + \sin(\varphi) \sin(\alpha\varphi) \\ \sin(\varphi) \cos(\alpha\varphi) - \cos(\varphi) \sin(\alpha\varphi) \end{pmatrix} \in \mathbb{R}^2.$$

For the numerical experiment we choose  $\alpha = 2/3$ . The Poisson problem then leads to  $U \notin H^2(\Omega)$ . Aitkin's  $\Delta^2$  method gives  $\|u\|^2 = 0.4041161973$ .

The initial coarse mesh  $\mathcal{T}_H^{(0)}$  with  $N = 8$  equisized elements and the corresponding discrete solution  $u_h$  for  $\ell = 4$  in Algorithm 6.1 as well as the exact solution are shown in Figure 4. Here,  $u$  and  $u_h$  are shown as plots over the arc length. The singularity of  $u$  at  $(0, 0)$  is visible at arc-length parameter  $s = 0$  and  $s = 2$  by periodicity.

To illustrate the performance of the proposed adaptive algorithm, we run Algorithm 6.1 with  $\mathcal{T}_0$  from Figure 4,  $\ell = 2, 3, 4$ , and  $\theta = 0, 1/2$ . The values of the error and the error estimators are visualized in Figures 5–7 and 9. The error  $E = \|u - u_h\|$  is computed via (7.1), where the energy norm of the exact solution is obtained by extrapolation with Aitkin's  $\Delta^2$  method,  $\|u\|^2 = 0.4041161973$ . For any choice of  $\ell$ , the uniform mesh refinement, i.e.,  $\theta = 0$ , leads to suboptimal convergence rate  $2/3$  for the error caused by a corner singularity of  $u$  which can be predicted theoretically. The fact that the slope of the corresponding error estimators even is  $2/3$  gives empirical evidence that the estimators are reliable and efficient although the solution lacks the regularity assumed in section 5. The error estimators  $\eta_M$  and  $\eta_A$ , respectively,  $\mu_M$  and  $\mu_A$  almost coincide. Due to numerical instabilities in computing the stiffness matrix for the  $\mathcal{P}_1$  boundary element method, the error estimators  $\mu_M$ ,  $\eta_M$ , and  $\eta_A$  are only computed up to an error of  $10^{-7/2}$ . Up to this breakdown of the computation, the  $\mu_M$ - and  $\mu_A$ -adaptive meshes coincide. Thus, for large numbers  $n$  of fine grid elements, Figures 5–7 only show the error and the error estimators  $\varrho_F$  and  $\mu_A$ .

The proposed adaptive mesh-refining strategy retains the optimal convergence rate  $3/2$  expected for smooth solutions; cf. section 7.1. This observation is independent of the choice of  $\ell$  in Algorithm 6.1. The larger  $\ell$ , the better is the estimation of the error by the error estimators  $\eta_A$  and  $\eta_M$  which can be expected from the involved constant  $L$  in Theorems 5.1 and 5.2; cf. (5.4) for the definition. We always have  $\eta_M \lesssim \|u - u_h\| \lesssim 1/(1 - L)\eta_M$ , where  $\lesssim$  denotes an inequality up to terms of higher order. By definition of our mesh strategy in Algorithm 6.1, there holds  $\|h\|_{L^\infty(\gamma_j)}/H_j = 1/\ell$ , whence  $L \rightarrow 0$  for  $\ell \rightarrow \infty$ . On the other hand,  $\ell$  should not be chosen too large since the asymptotic behavior of  $h^{3/2}$  and  $H^{5/2}$  then might not be visible for the number of elements considered. However, the effect is visible for  $\ell = 2, 3, 4$  as well; cf. Figures 5–7. For  $\ell = 2$ , the curves of  $\eta_M$ ,  $\eta_A$ , and  $E$  are getting closer for  $H, h \rightarrow 0$ , and it is expected that the curves almost coincide for larger values of  $n$ . For  $\ell = 3$ , the error and the error estimators  $\eta_M$  and  $\eta_A$  seem to coincide for  $n \geq 200$ . Finally, for  $\ell = 4$ , the error is sharply estimated by  $\eta_M$  and  $\eta_A$  even for lower degrees of freedom; cf. Figure 7.

Figure 8 shows the sequence of ( $\mu_A$ -) adaptively generated meshes  $\mathcal{T}_H$ . We observe the expected mesh refinement towards the reentrant corner at the endpoints 0 and 2 and a moderate refinement elsewhere. The sequence of adaptive meshes for  $\ell = 2, 3$  looks similar. Figure 9 shows the error and the error estimator  $\mu_A$  for uniform and  $\mu_A$ -adaptive mesh refinement and, for comparison,  $\ell = 2, 3, 4$ . Note that not only the slope of the errors for different choices of  $\ell$  but even the absolute values coincide asymptotically.

Finally, Table 3 shows the calculated values of the error  $E = \|u - u_h\|$ , the error estimator, and the corresponding experimental convergence rate  $\kappa$  for uniform and  $\mu_A$ -adaptive mesh refinement and  $\ell = 4$ . The values underline the given interpretation of the figures. For uniform mesh refinement,  $\mu_A$  overestimates the error by a factor 2.75 independent of the number  $n$  of fine grid elements. For adaptively generated meshes, the quotient  $\mu_A/E$  varies between 2.75 and 5 and seems to converge to a value about 3 for large  $n$ . This underlines the empirical efficiency and reliability of  $\mu_A$  as is proven for smooth solutions in section 5. For the error estimators  $\mu_M$  and  $\mu_A$ , the quotient  $\mu_M/\mu_A$  is about 1 and both error estimators almost coincide. This underlines why both refinement strategies lead to the same adaptive mesh refinement.

**7.3. Symm's integral equation with constant right-hand side.** The boundary integral equation  $V\phi = 1$  with constant right-hand side is considered for the L-

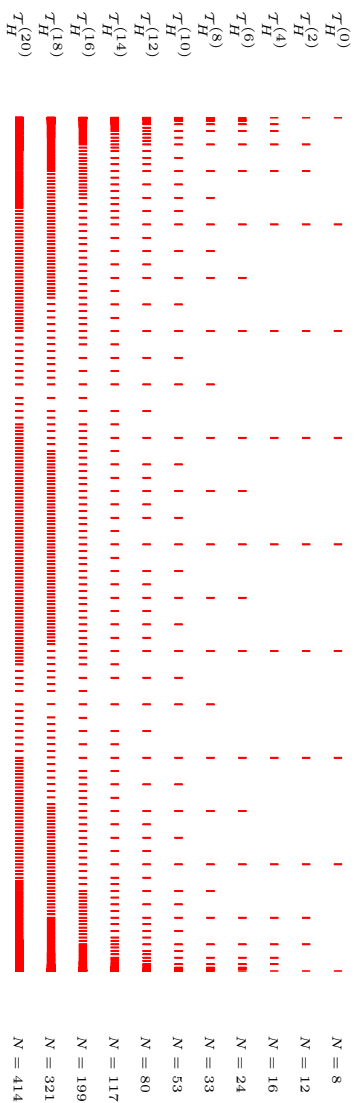


FIG. 8. Adaptive mesh refinement in Poisson problem 7.2 related to  $\ell = 4$  and error estimator  $\mu_A$ . Adaptive mesh-refinement with respect to  $\mu_N$  leads to the same meshes up to  $T_H^{(11)}$  [with  $N = 64$  coarse grid elements] when the P1 boundary element method becomes unstable. The adaptively generated meshes are highly adapted towards the reentrant corner of the L-shape.

TABLE 3

Experimental error, error estimator  $\mu_A$ , and convergence rates for Poisson problem 7.2,  $\ell = 4$ , and uniform (top), respectively,  $\mu_A$ -adaptive mesh refinement (bottom).

Uniform mesh refinement						
$k$	$n$	$E$	$\mu_A$	$\mu_A/E$	$\mu_A/\mu_M$	$\kappa$
0	32	4.5341e-02	1.2451e-01	2.75	0.979	
1	64	2.8567e-02	7.8630e-02	2.75	0.984	0.67
2	128	1.7999e-02	4.9539e-02	2.75	0.984	0.67
3	256	1.1339e-02	3.1211e-02	2.75	0.984	0.67
4	512	7.1434e-03	1.9662e-02	2.75	0.984	0.67
5	1024	4.5001e-03	1.2387e-02	2.75	0.984	0.67
6	2048	2.8349e-03	7.8032e-03	2.75	n/a	0.67
Adaptive mesh refinement						
$k$	$n$	$E$	$\mu_A$	$\mu_A/E$	$\mu_A/\mu_M$	$\kappa$
0	32	4.5341e-02	1.2451e-01	2.75	0.979	
2	48	1.8094e-02	5.0731e-02	2.80	0.984	2.51
4	64	7.4020e-03	2.2723e-02	3.07	0.984	3.30
6	96	3.0431e-03	1.0351e-02	3.40	0.983	1.66
8	132	1.3706e-03	5.4421e-03	3.97	0.988	1.79
10	212	5.7738e-04	2.4396e-03	4.23	0.986	2.01
12	320	2.6589e-04	1.2230e-03	4.60	n/a	1.65
14	468	1.2698e-04	6.3510e-04	5.00	n/a	1.76
16	796	7.1773e-05	2.6601e-04	3.71	n/a	1.62
18	1284	3.8295e-05	1.3110e-04	3.42	n/a	1.15
20	1656	2.8272e-05	8.6995e-05	3.08	n/a	1.33

shaped domain  $\Omega$  of Figure 4. To compute the error in the energy norm, we used the extrapolated value  $\|u\|^2 = 2.40769127$  in (7.1). The exact solution  $u$  is unknown. Figure 10 shows discrete solutions  $u_h$  related to the initial mesh and an adaptively generated mesh [with  $n = 32$  and  $n = 656$  fine grid elements, resp.]. The discrete solutions show singularities at the five rectangular corners of the L-shape corresponding to the arc-length parameters  $s = 1/4, 1/2, 1, 3/2$ , and  $7/4$ . Figure 11 shows the errors and the error estimators for uniform and  $\mu_A$ -adaptive mesh refinement and  $\ell = 3, 4$  in Algorithm 6.1. As in Poisson problem 7.2, the error is sharply estimated by the error estimators  $\eta_M$  and  $\eta_A$  and the error estimators  $\mu_M$  and  $\mu_A$  coincide: The larger  $\ell$ , the better is the error estimation. Again, the  $\mathcal{P}_1$  boundary element stiffness matrix showed instabilities for the error  $E \approx 10^{-7/2}$ . The corresponding adaptive meshes are shown in Figure 12.

**7.4. Exterior crack problem with nonsmooth solution.** The fourth example from [ChS] represents a typical endpoint singularity for open curves and concerns the Poisson problem (6.2) exterior to a straight slit  $\Gamma := [-1, 1] \times \{0\}$ ,  $\Omega := \mathbb{R}^2 \setminus \Gamma$ . For  $g(x, 0) := -x$ , the exact solution  $u$  of the corresponding Symm's integral equation reads

$$(7.9) \quad u(x, 0) = -x/\sqrt{1-x^2} \quad \text{for } -1 < x < 1.$$

There holds  $u \in H^\alpha(\Gamma)$  for all  $\alpha < 0$ , but  $u \notin L^2(\Gamma)$  since  $u$  is singular at the tips of the domain,  $u(x, 0) \rightarrow \pm\infty$  for  $x \rightarrow \pm 1$ . Since  $Kg$  vanishes on the straight slit  $\Gamma$ , Symm's integral equation (1.1) simplifies to

$$(7.10) \quad Vu = g \quad \text{on } \Gamma.$$

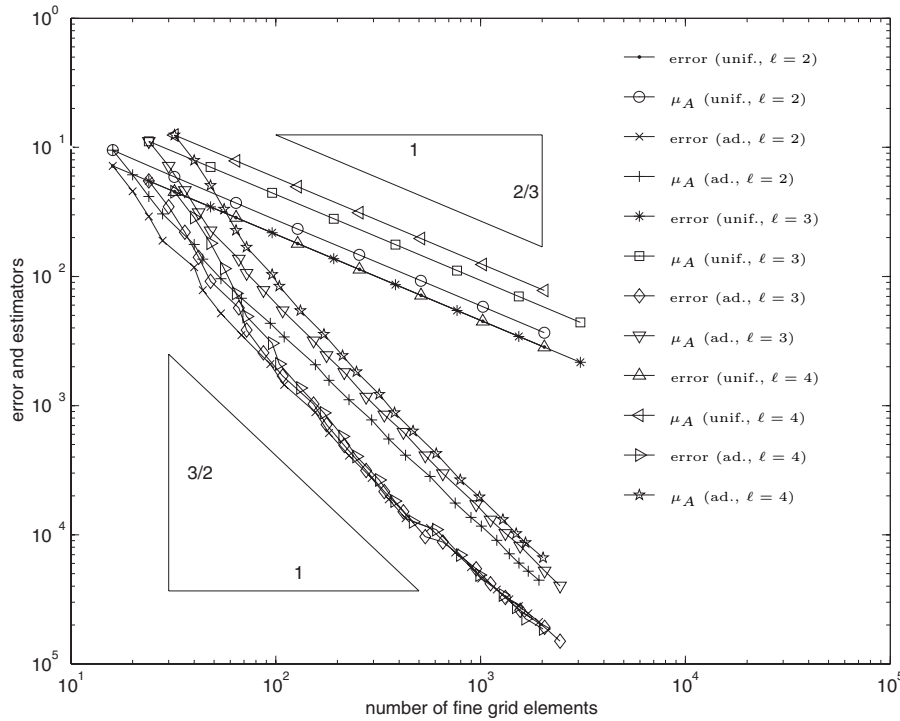


FIG. 9. Comparison of error and error estimator  $\mu_A$  in Poisson problem 7.2 for uniform and  $\mu_A$ -adaptive mesh refinement and different choices of  $\ell = 2, 3, 4$  in Algorithm 6.1.

The energy norm of the exact solution can be computed exactly,

$$\|u\|^2 = \langle Vu; u \rangle = \int_{-1}^1 \frac{x^2}{\sqrt{1-x^2}} dx = \frac{\pi}{2}.$$

Figure 13 shows the error and error estimators for  $\ell = 3, 4$  and both uniform and adaptive mesh refinement. Some adaptively generated meshes are provided in Figure 14. As can be expected, we observe a high mesh refinement towards the ends  $\pm 1$  of the slit and coarse local mesh sizes inbetween.

**7.5. Smooth eigenfunction of the single-layer potential.** Finally, we consider an example on a smooth boundary with the discrete scheme involving the approximation of the boundary  $\Gamma$  by a piecewise-affine boundary  $\Gamma_h$ . Note that the error due to the boundary approximation is not included in the analysis given above.

We consider the sphere  $\Gamma = \partial B(0, r)$  with radius  $r < 1$ . Then, for fixed  $k \in \mathbb{Z} \setminus \{0\}$ ,

$$(7.11) \quad \phi(x) := \cos(kt) \quad \text{with } x = r(\cos t, \sin t)$$

is an eigenfunction of the single-layer potential  $V$  corresponding to the eigenvalue  $\lambda = r/|k|$ . For the numerical experiment, we used  $r = 1/2$  and  $k = 3$ . Note that this example satisfies the smoothness assumptions of section 5. For the implementational realization, we approximate  $\Gamma$  by a (convex) polygonal  $\Gamma_H$  with vertices on the sphere. We therefore modify the adaptive Algorithm 6.1 as follows.

ALGORITHM 7.1. Choose an initial mesh  $\mathcal{T}_H^{(0)}$  consisting of affine boundary pieces such that all nodes of  $\mathcal{T}_H^{(0)}$  are on the sphere. Let  $k = 0$ ,  $\ell \in \mathbb{N}_{\geq 2}$ , and  $0 \leq \theta \leq 1$ .

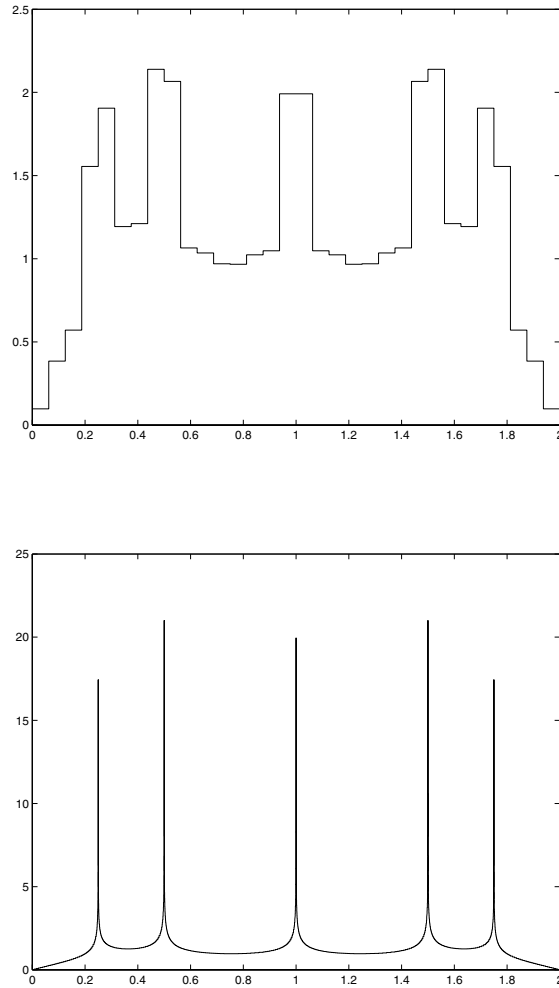


FIG. 10. Discrete solution  $u_h$  ( $n = 32$ ) in Example 7.3 related to  $\ell = 4$  and the initial mesh  $\mathcal{T}_H^{(0)}$  with  $N = 8$  elements shown in Figure 4 (top) and discrete solution  $u_h$  ( $n = 656$ ) related to  $\mu_A$ -adaptive generated coarse mesh  $\mathcal{T}_H^{(10)}$  with  $N = 164$  elements (bottom). Note the different scalings on the y-axis of the plots.

- (i) Obtain  $\mathcal{T}_h^{(k)} = \{\Gamma_1, \dots, \Gamma_n\}$  from  $\mathcal{T}_H^{(k)} = \{\gamma_1, \dots, \gamma_N\}$  by uniform splitting of each element  $\gamma_j \in \mathcal{T}_H^{(k)}$  into  $\ell$  elements of equal length.
- (ii) Create a further mesh  $\tilde{\mathcal{T}}_h^{(k)}$  by mapping all nodes of  $\mathcal{T}_h^{(k)}$  onto the sphere.
- (iii) Compute the discrete solution  $\tilde{u}_h^{(k)}$  for the mesh  $\tilde{\mathcal{T}}_h^{(k)}$ .
- (iv) Since each element  $\Gamma_j \in \mathcal{T}_h^{(k)}$  corresponds to exactly one element  $\tilde{\Gamma}_j \in \mathcal{T}_h^{(k)}$  with nodes on the sphere, we may define  $u_h \in \mathcal{P}_0(\mathcal{T}_h^{(k)})$  by  $u_h|_{\Gamma_j} := \tilde{u}_h|_{\tilde{\Gamma}_j}$  for all  $\Gamma_j \in \mathcal{T}_h^{(k)}$ .
- (v) Compute error estimators  $\eta_M$  and  $\eta_A$  and refinement indicators  $\mu_{M,j}$  and  $\mu_{A,j}$ .

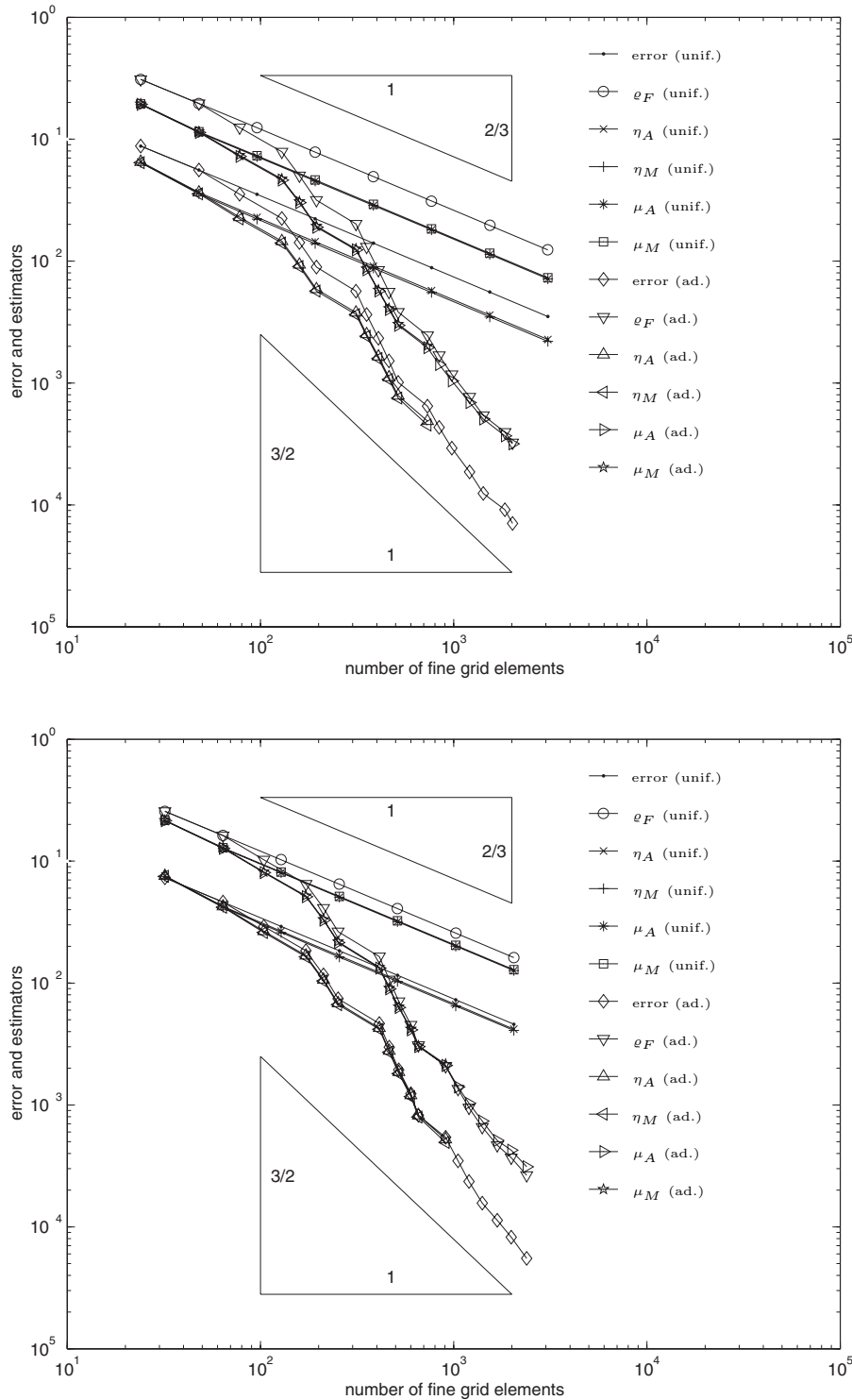


FIG. 11. Error and error estimators  $\eta_M$ ,  $\eta_A$ ,  $\mu_M$ , and  $\mu_A$  for uniform [indicated by unif.] and  $\mu_A$ -adaptive [indicated by ad.] mesh refinement in Example 7.3 and  $\ell = 3$  (top), respectively,  $\ell = 4$  (bottom) in Algorithm 6.1. As for Poisson problem 7.2, the larger  $\ell$ , the sharper is the error estimated by the error estimators  $\eta_M$  and  $\eta_A$ . On the other hand, the larger  $\ell$ , the larger is the presymptotic range before the optimal convergence order  $3/2$  is visible for adaptive mesh refinement.

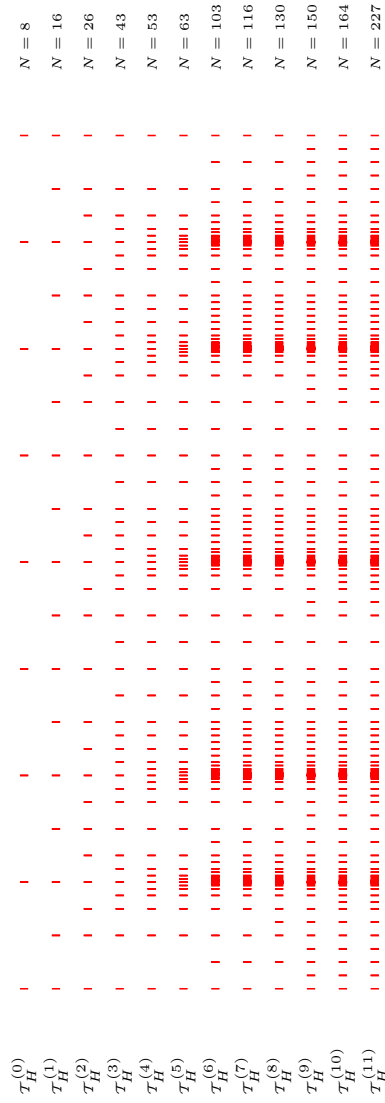


FIG. 12. Adaptive mesh refinement in Example 7.3 related to  $\ell = 4$  and error estimator  $\mu_A$ . Adaptive mesh refinement with respect to  $\mu_M$  leads to the same meshes up to  $T_H^{(11)}$  [with  $N = 64$  coarse grid elements] when the P1 boundary element method becomes unstable. The adaptively generated meshes are highly adapted towards the five rectangular corners of the L-shape, where the discrete solutions show singularities; cf. Figure 10.

- (vi) Mark element  $\gamma_j \in \mathcal{T}_H^{(k)}$  provided the corresponding refinement estimator satisfies  $\mu_{M,j} \geq \theta \max\{\mu_{M,1}, \dots, \mu_{M,N}\}$  and  $\mu_{A,j} \geq \theta \max\{\mu_{A,1}, \dots, \mu_{A,N}\}$ , respectively.
- (vii) Halve all marked elements  $\gamma_j \in \mathcal{T}_H^{(k)}$ , map the new nodes onto the sphere, and so generate a new coarse mesh  $\mathcal{T}_H^{(k+1)}$ , update  $k$ , and go to (i).

To clarify the mesh organization, Figure 15 shows the initial coarse mesh with  $N = 6$  elements and the refined meshes  $\mathcal{T}_h^{(0)}$  and  $\tilde{\mathcal{T}}_h^{(0)}$  for  $\ell = 3$  with  $n = 18$  elements. Experimental results are shown in Figure 16 for  $\ell = 4$  and both uniform and adaptive mesh refinement. As can be expected from the smoothness of  $u$ , the adaptive mesh refining strategy leads to almost uniform meshes. The experimental convergence orders for uniform and adaptive mesh refinement stay optimal. The curves of the error and error estimators almost coincide.

**8. Conclusions.** In this paper we introduced a new class of error estimators based on averaging techniques. We gave the analytical fundament that these error estimators estimate the (unknown) error  $\|u - u_h\|$  both reliably and efficiently, under weak assumptions on the boundary elements used. The strongest assumption is a (piecewise) high regularity of the exact solution  $u$ . However, this regularity assumption might be nonsatisfied in practice. We introduced an adaptive algorithm which steers the mesh refinement with respect to the localized error estimators  $\mu_M$  and  $\mu_A$ , respectively. In the numerical experiments we treated examples with different regularity. In all experiments the introduced adaptive strategy retains the optimal convergence rate  $\mathcal{O}(h^{3/2})$  and is therefore superior to uniform mesh refinement.

Finally, we highlight some of our computational and analytical results.

**8.1. Error estimation with  $\eta_M$ ,  $\eta_A$  and choice of  $\ell$ .** The numerical experiments underline the good performance of the introduced error estimators. The values of the error estimators  $\eta_M$  and  $\eta_A$  almost coincide with the error  $\|u - u_h\|$  provided  $\ell$  is chose large enough. The explicit choice of  $\ell$  is not discussed in this paper and is part of a generalized eigenvalue problem to compute  $C_{\Pi} C_{\text{inv}}^{H,q}$  in (5.4). For the numerical experiments treated, the choice of  $\ell = 3, 4$  was sufficient to ensure that the error is sharply estimated by  $\eta_M$  and  $\eta_A$ . The efficiency and reliability constants, i.e.,

$$C_{\text{eff}}^{-1} \eta \leq \|u - u_h\| \leq C_{\text{rel}} \eta$$

for an error estimator  $\eta$ , are unknown except that we know  $C_{\text{eff}} = 1$  [up to higher order terms] for  $\eta_M$ . At least in the numerical experiments in section 7 we observed  $C_{\text{eff}}, C_{\text{rel}} \rightarrow 1$  for  $h \rightarrow 0$ .

**8.2. Adaptive mesh-refinement with respect to  $\mu_M$ ,  $\mu_A$ .** The examples 7.2–7.4 show that the proposed adaptive strategy can retain the optimal convergence rate  $\mathcal{O}(h^{3/2})$  even for examples with nonsmooth exact solution. Poisson problem 7.2, also a benchmark for 2D finite element schemes, has exactly one corner singularity. Therefore the asymptotic convergence rates are visible from the beginning. This is not typical and so we addressed a generic example with smooth right-hand side, namely  $f = 1$ , which is [according to the authors' knowledge] not explicitly accompanied with an equivalent Poisson problem. Figure 11 shows a larger preasymptotic range for  $N \leq 20$  and adaptive mesh refinement. The final Example 7.5 shows how the averaging based error estimation can be employed in combination with the approximation of a smooth boundary.

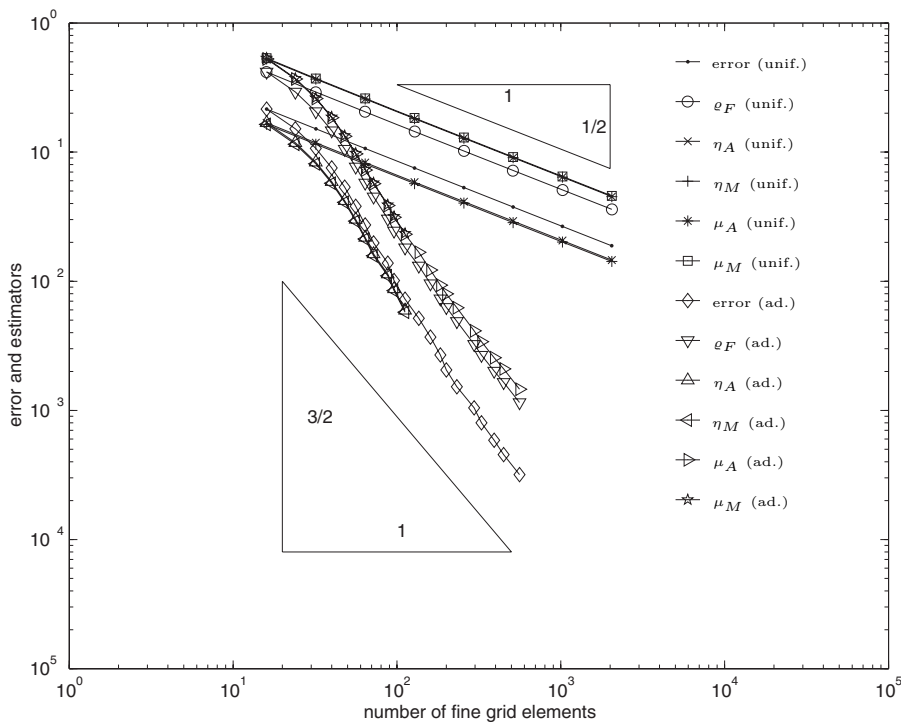
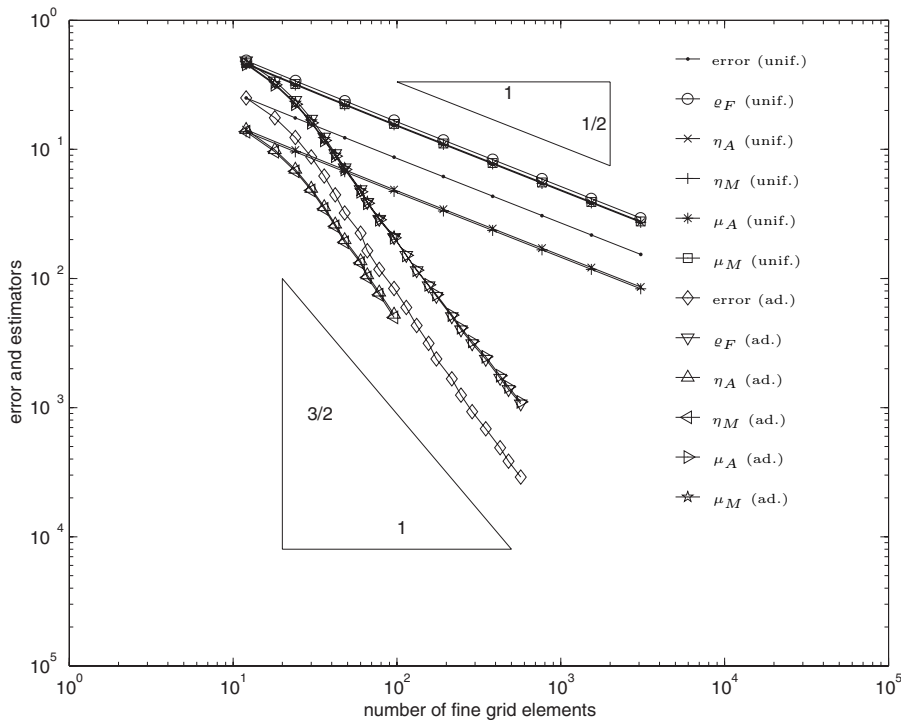


FIG. 13. Error and error estimators  $\eta_M$ ,  $\eta_A$ ,  $\mu_M$ , and  $\mu_A$  for uniform [indicated by unif.] and  $\mu_A$ -adaptive [indicated by ad.] mesh refinement in Example 7.4 and  $\ell = 3$  (top), respectively,  $\ell = 4$  (bottom) in Algorithm 6.1.

**8.3. Computational cost of the introduced error estimators.** The naive computational cost for the estimators  $\mu_M$ ,  $\eta_M$ ,  $\eta_A$  is quadratic in the number of unknowns since we have to compute the stiffness matrix for the  $\mathcal{P}_1$  boundary element methods to compute  $\mathbb{G}_H u_h$  for  $\mu_M$  and  $\eta_M$ , respectively,  $\|\mathbb{G}_H u_h\|$  and  $\|\mathcal{A}_H u_h\|$  for  $\eta_M$  and  $\eta_A$ . This can be overcome by use of approximation techniques like panel clustering or  $\mathcal{H}$ -matrices which compute, store, and evaluate the stiffness matrix in almost linear complexity. Nevertheless, the computational cost for computing  $\mu_A$  seems to be striking: The computation of  $\mu_A$  for the  $L^2$ -projection  $\mathcal{A}_H$  only needs the assembly of the usual  $L^2$  mass matrix  $\mathbf{M}$ . This matrix is sparse and therefore assembled and stored in linear complexity. Moreover, the computation of  $\mathcal{A}_H u_h$  involves the solution of  $\mathbf{M}\mathbf{y} = \mathbf{c}$  for a given right-hand side  $\mathbf{c}$ , and the condition number of  $\mathbf{M}$  is bounded, i.e.,  $\mathcal{O}(1)$  for  $h \rightarrow 0$ .

**8.4. Applicability to 3D problems.** We stress that the presented analysis works for 3D problems, i.e., 2D boundary pieces, as well. In the numerical experiments we restricted ourselves to 2D problems for ease of presentation, since the implementation of the boundary element schemes and even the data structures are much more involved for the 3D boundary element method.

**8.5. Further developments and open problems.** From an analytical point of view, Theorem 5.1 is the core result for providing the averaging error estimators. The proof is only based on the validity of a local inverse estimate; cf. section 3.2, and the existence of an appropriate (local) first order approximation operator. In a forthcoming paper, we will provide both the hypersingular integral equation as well [CP2, FP]. It is expected that the ideas carry over to a quite general class of integral equations.

The analytical verification of the introduced error estimators needs high regularity assumptions on  $u$ . Since our numerical experiments indicate that these assumptions can be weakened, it would be desirable to have a refined analysis that covers these cases as well, i.e. which either avoids the regularity assumptions on  $u$  or explains the good performance of the indicator-based strategy analytically.

#### REFERENCES

- [AC] J. ALBERTY AND C. CARSTENSEN, *Averaging techniques for reliable a posteriori FE-error control in elastoplasticity with hardening*, Comput. Methods Appl. Mech. Engrg., 192 (2003), pp. 1435–1450.
- [BL] J. BERGH AND J. LÖFSTRÖM, *Interpolation Spaces*, Grundlehren der Mathematischen Wissenschaften 223, Springer-Verlag, Berlin, 1976.
- [BR] I. BABUŠKA AND W. C. RHEINOLDT, *Error estimates for adaptive finite element computations*, SIAM J. Numer. Anal., 15 (1978), pp. 736–754.
- [C1] C. CARSTENSEN, *Adaptive boundary element methods and adaptive finite element and boundary element coupling*, In *Boundary value problems and integral equations on non-smooth domains*. Lecture Notes in Pure and Applied Mathematics 167, M. Costabel, M. Dauge, S. Nicaise, eds., Marcel Dekker, New York (1995), pp. 47–58.
- [C2] C. CARSTENSEN, *Efficiency of a posteriori BEM-error estimates for first kind integral equations on quasi-uniform meshes*, Math. Comp., 65 (1996), pp. 69–84.
- [C3] C. CARSTENSEN, *An a posteriori error estimate for a first-kind integral equation*, Math. Comp., 66 (1997), pp. 139–155.
- [CB] C. CARSTENSEN AND S. BARTELS, *Each averaging technique yields reliable a posteriori error control in FEM on unstructured grids. I. Low order conforming, nonconforming, and mixed FEM*, Math. Comp., 71 (2002), pp. 945–969.
- [CES] C. CARSTENSEN, D. ESTEP, AND E. P. STEPHAN, *h-adaptive boundary element schemes*, Comput. Mech., 15 (1995), pp. 372–383.

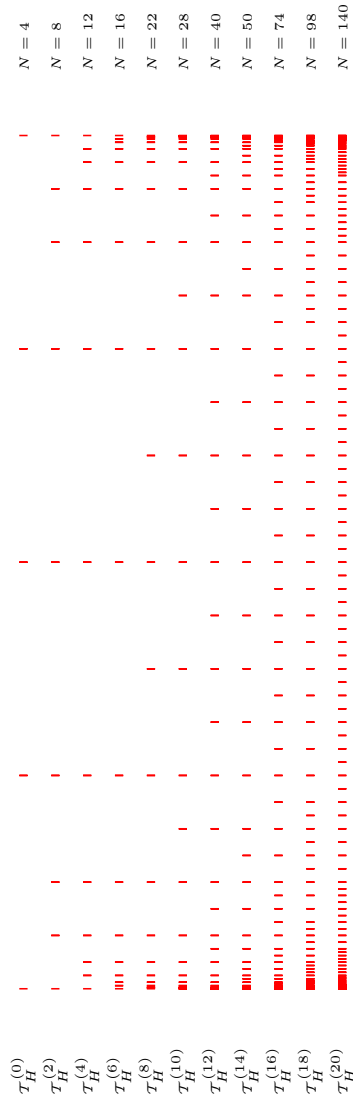


FIG. 14. Adaptive mesh refinement in slit Problem 7.4 related to  $\ell = 4$  and error estimator  $\mu_A$ . Adaptive mesh refinement with respect to  $\mu_M$  leads to the same meshes up to  $\mathcal{T}_H^{(11)}$  [with  $N = 64$  coarse grid elements] when the P1 boundary element method becomes unstable. The adaptively generated meshes are highly adapted towards the endpoints  $(\pm 1, 0)$  of the slit.

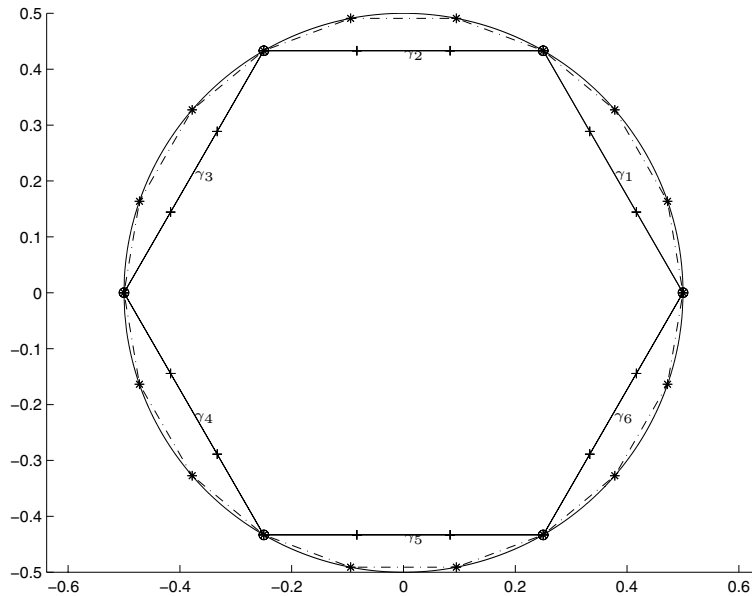


FIG. 15. *Initial meshes in Example 7.5: The initial coarse mesh  $\mathcal{T}_H^{(0)}$  consists of  $N = 6$  elements [nodes marked by  $\circ$ ]. For  $\ell = 3$ ,  $\mathcal{T}_h^{(0)}$  is a refinement of  $\mathcal{T}_H^{(0)}$  with  $n = 18$  elements [nodes marked by  $+$ ] and  $\tilde{\mathcal{T}}_h^{(0)}$  is obtained by projecting the nodes onto the sphere [marked by  $*$ ].*

- [CFa] C. CARSTENSEN AND B. FAERMANN, *Mathematical foundation of a posteriori error estimates and adaptive mesh-refining algorithms for boundary integral equations of the first kind*, Eng. Anal. Bound. Elem., 25 (2001), pp. 497–509.
- [CFu] C. CARSTENSEN AND S. A. FUNKEN, *Averaging technique for FE—a posteriori error control in elasticity. I. Conforming FEM*, Comput. Methods Appl. Mech. Eng., 190 (2001), pp. 2483–2498. II.  $\lambda$ -independent estimates, Comput. Methods Appl. Mech. Eng., 190 (2001), pp. 4663–4675. III. *Locking-free nonconforming FEM*, Comput. Methods Appl. Mech. Eng., 191 (2001), pp. 861–877.
- [CFS] C. CARSTENSEN, S. A. FUNKEN, AND E. P. STEPHAN, *A posteriori error estimates for hp-boundary element methods*, Appl. Anal., 61 (1996), pp. 233–253.
- [CMS] C. CARSTENSEN, M. MAISCHAK, AND E. P. STEPHAN, *A posteriori error estimate and h-adaptive algorithm on surfaces for Symm’s integral equation*, Numer. Math., 90 (2001), pp. 197–213.
- [CMPS] C. CARSTENSEN, M. MAISCHAK, D. PRAETORIUS, AND E. P. STEPHAN, *Residual-based a posteriori error estimate for hypersingular equation on surfaces*, Numer. Math., 97 (2004), pp. 397–425.
- [CP1] C. CARSTENSEN AND D. PRAETORIUS, *A posteriori error control in adaptive quadrature boundary element analysis for a logarithmic-kernel integral equation of the first kind*, SIAM J. Sci. Comput., 25 (2003), pp. 259–283.
- [CP2] C. CARSTENSEN AND D. PRAETORIUS, *Averaging techniques for the a posteriori BEM error control for a hypersingular integral equation in 2d*, SIAM J. Sci. Comp., accepted, 2005.
- [CS1] C. CARSTENSEN AND E. P. STEPHAN, *A posteriori error estimates for boundary element methods*, Math. Comput., 64 (1995), pp. 483–500.
- [CS2] C. CARSTENSEN AND E. P. STEPHAN, *Adaptive boundary element methods for some first kind integral equations*, SIAM J. Numer. Anal., 33 (1996), pp. 2166–2183.
- [ChS] G. A. CHANDLER AND I. H. SLOAN, *Spline quadrature methods for boundary integral equations*, Numer. Math., 58 (1990), pp. 537–567.
- [Co] M. COSTABEL, *Boundary integral operators on Lipschitz domains: Elementary results*, SIAM J. Math. Anal., 19 (1988), pp. 613–626.

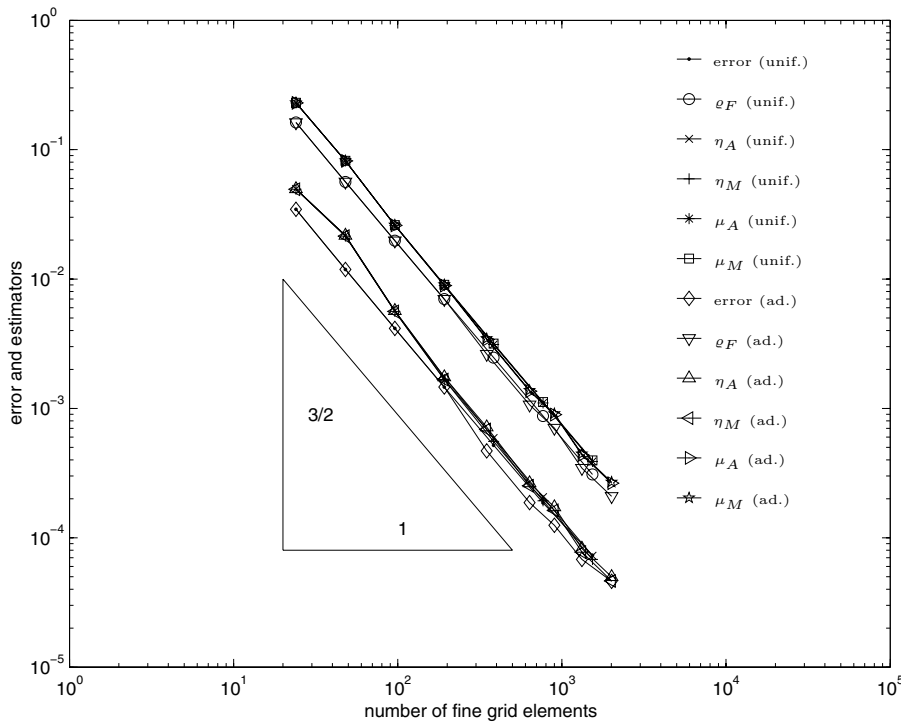


FIG. 16. Error and error estimators  $\eta_M$ ,  $\eta_A$ ,  $\mu_M$ , and  $\mu_A$  for uniform [indicated by unif.] and  $\mu_A$ -adaptive [indicated by ad.] mesh refinement in Example 7.5 and  $\ell = 4$  in Algorithm 6.1.

- [F1] B. FAERMANN, *Local a-posteriori error indicators for the Galerkin discretization of boundary integral equations*, Numer. Math., 79 (1998), pp. 43–76.
- [F2] B. FAERMANN, *Localization of the Aronszajn-Slobodeckij norm and application to adaptive boundary element methods. I. The two-dimensional case*, IMA J. Numer. Anal., 20 (2000), pp. 203–234.
- [F3] B. FAERMANN, *Localization of the Aronszajn-Slobodeckij norm and application to adaptive boundary element methods. II. The three-dimensional case*, Numer. Math., 92 (2002), pp. 467–499.
- [FHK] M. FEISTAUER, G. C. HSIAO, AND R. E. KLEINMAN, *Asymptotic and a posteriori error estimates for boundary element solutions of hypersingular integral equations*, SIAM J. Numer. Anal., 33 (1996), pp. 666–685.
- [FP] S. FUNKEN AND D. PRAETORIUS, *Averaging on large patches for first kind integral equations in 3D*, work in progress, 2005.
- [GHS] I. G. GRAHAM, W. HACKBUSCH, AND S. A. SAUTER, *Finite elements on degenerate meshes: Inverse-type inequalities and applications*, IMA J. Numer. Anal., 25 (2005), pp. 379–407.
- [HMS] N. HEUER, M. MAISCHAK, AND E. P. STEPHAN, *Exponential convergence of the hp-version for the boundary element method on open surfaces*, Numer. Math., 83 (1999), pp. 641–666.
- [Ma] M. MAISCHAK, *The Analytical Computation of the Galerkin Elements for the Laplace, Lamé and Helmholtz Equation in BEM*, Preprint (1999): 2D BEM, Preprint (2000): 3D BEM, Institut für Angewandte Mathematik, Universität Hannover.
- [MMS] M. MAISCHAK, P. MUND, AND E. P. STEPHAN, *Adaptive multilevel BEM for acoustic scattering*, Comput. Methods Appl. Mech. Engrg., 150 (1997), pp. 351–367.
- [McL] W. MCLEAN, *Strongly Elliptic Systems and Boundary Integral Equations*, Cambridge University Press, Cambridge, UK, 2000.

- [MPM] G. MENON, G. H. PAULINO, AND S. MUKHERJEE, *Analysis of hypersingular residual error estimates in boundary element methods for potential problems*, *Comput. Methods Appl. Mech. Engrg.*, 73 (1999), pp. 449–473.
- [MSW] P. MUND, E. P. STEPHAN, AND J. WEISSE, *Two-level methods for the single-layer potential in  $\mathbb{R}^3$* , *Computing*, 60 (1998), pp. 243–266.
- [P] T. VON PETERSDORFF, *Randwertprobleme der Elastizitätstheorie für Polyeder–Singularitäten und Approximation mit Randelementmethoden*, PhD thesis, Darmstadt, Germany, 1989.
- [R1] E. RANK, *A-posteriori error estimates and adaptive refinement for some boundary integral element method*, in *Proc. Int. Conf. on Accuracy Estimates and Adaptive Refinements in FE Computations ARFEC*, Lisbon, Portugal, 1984, pp. 55–64.
- [R2] E. RANK, *Adaptivity and accuracy estimation for FEM and BEM*, in *Accuracy Estimates and Adaptive Refinements in FE Computations*, I. Babuška, O. C. Zienkiewicz, J. Gago, E. R. Oliveira, eds., Wiley, Chichester, UK, 1986.
- [SaS] S. A. SAUTER AND C. SCHWAB, *Randelemente, Analyse und Implementierung Schneller Algorithmen*, Teubner, Stuttgart, Germany, 2004.
- [SSW] H. SCHULZ, C. SCHWAB, AND W. L. WENDLAND, *Extraction, higher order boundary element methods, and adaptivity*, in *Mathematical aspects of boundary element methods* (Palaiseau, 1998), *Chapman & Hall/CRC Res. Notes Math.*, 414, Chapman & Hall/CRC, Boca Raton, FL 2000, pp. 263–274.
- [SSt] H. SCHULZ AND O. STEINBACH, *A new a posteriori error estimator in adaptive direct boundary element methods. The Dirichlet problem*, *Calcolo*, 37 (2000), pp. 79–96.
- [SW] C. SCHWAB AND W. L. WENDLAND, *On the extraction technique in boundary integral equations*, *Math. Comp.*, 68 (1999), pp. 91–122.
- [S] O. STEINBACH, *Adaptive boundary element methods based on computational schemes for Sobolev norms*, *SIAM J. Sci. Comput.*, 22 (2000), pp. 604–616.
- [StS] E. P. STEPHAN AND M. SURI, *The h-p version of the boundary element method on polygonal domains with quasiuniform meshes*, *RAIRO Model. Math. Anal. Numér.*, 25 (1991), pp. 783–807.
- [WY] W. L. WENDLAND AND D. YU, *Adaptive boundary element methods for strongly elliptic integral equations*, *Numer. Math.*, 53 (1988), pp. 539–558.
- [Y1] D. YU, *A posteriori error estimates and adaptive approaches for some boundary element methods*, in *Boundary Elements 9*, C. A. Brebbia, W. L. Wendland, G. Kuhn, eds., Berlin, Stuttgart, (1987), pp. 241–256.
- [Y2] D. YU, *Self-adaptive boundary element methods*, *ZAMM*, 68 (1988), pp. T435–T437.
- [ZZ] O. C. ZIENKIEWICZ AND J. Z. ZHU, *A simple error estimator and adaptive procedure for practical engineering analysis*, *Internat. J. Numer. Methods Engrg.*, 24 (1987), pp. 337–357.